BNL-228983-2025-TECH

CA/AP/725

Space Charge Simulations of High Intensity Proton Beams in the AGS Booster

J. Beebe-Wang

September 2025

Collider Accelerator Department

Brookhaven National Laboratory

U.S. Department of Energy

USDOE Office of Science (SC), Nuclear Physics (NP)

DISCLAIMER

Space Charge Simulations of High Intensity Proton Beams in the AGS Booster

Joanne Beebe-Wang

September 2025

Contents

1 Introduction

Computer simulation studies have been performed to understand the beam behavior and to explore intensity limitations of proton beams in the AGS Booster at higher beam intensities. During the 100 GeV polarized proton operations of RHIC Run 2024, sPHENIX operated in modes with a crossing angle at collisions in order to mitigate beam-beam effects. Three different running modes were employed:

(a) sPHENIX operated with a negative (-2 mrad) crossing angle, and STAR operated with 0 mrad. Both experiments were brought into collisions at the start of the store.

(b) sPHENIX was brought into collisions with 0 mrad first. Then STAR was brought into collisions after the beam-beam parameter from sPHENIX reduced to below 10×10^{-3}.

(c) sPHENIX operated with a positive (+1.5 mrad) crossing angle, and STAR operated with 0 mrad. Both experiments were brought into collisions at the start of the store.

The collisions with a crossing angle of up to ± 2 mrad, as in running modes (a) and (c), lead to large Piwinski angle in the new sPHENIX detector, which reduces luminosity if other parameters are unchanged. There are two ways to compensate the reduction in luminosity: squeeze β^* if there is sufficient dynamic aperture, or increase the injected beam intensity. The first part of polarized proton operation during RHIC Run 2024 was dedicated to increasing the intensity. Different configurations were tested with crossing angle and lattice adjustments on RHIC. At the same time, new injector configurations were developed and tested in an effort to push for both higher intensity and better quality of the beam injected into RHIC.

When the beam intensity is increased, space charge is a concern particularly in the lower energy stages of acceleration, such as during the injection and the early part of the Booster cycle, which could become a dominant effect in limiting the intensity of the beam that can be delivered to RHIC.

One approach to such a study is to include calculations of space charge in computer simulation codes that track the motion of charged particles in 6D phase space [1]. Unfortunately, repeated space charge calculations in 6D phase space are computationally intensive even with the most modern computing facilities. Study with traditional models of space charge is then either limited to a short real-time scale, or sacrifices accuracy and often omits some of the physics.

The description of two models traditionally used for space charge calculation and the introduction of an alternative, the hybrid model, that is applicable to these studies is presented in [2]. The features of a code necessary to realistically simulate beams in the AGS Booster, as well as the justification for choosing "`Simpsons`" [3] as the simulation code for this study can be found in Section 3 of [2].

The simulation studies are performed for the full cycle of injection, RF capture and energy ramping in the AGS Booster in the presence of space charge. Optimizations have been carried out at various stages of the Booster cycle covering features such as injection, beam bunching, and tune ramping. The numerical parameters are determined through comparison and examination of the results of a large number of test simulations. Their impact on the accuracy of simulation results and the required CPU times can be found in Section 4 of [2].

The focus of this report is on issues directly related to space-charge in high intensity proton beams, mainly as a result of emittance increase in the transverse and/or longitudinal planes. Detailed studies distinguishing between linear and non-linear space charge effects, identifying image charge effects from direct Coulomb interactions, exploring parameters pushed to the onset of higher order resonance, and examining impedance effects and beam halo formation, are not included.

2 Simulation Model and Parameters

2.1 Accelerator Model of the AGS Booster

The magnets, primary RF and higher harmonic RF cavities, beam monitoring elements and other machine elements are based on the standard `MADX` model of the AGS Booster. The Booster lattice description was converted from `MADX` format into the inputs for `Simpsons` simulations, supplying details of machine optics and lattice parameters at all elements around the Booster ring.

Some modifications and adjustments to the standard Booster model are achieved through re-calculating and modifying the strengths and parameters of elements for the whole ring. Each simulation run with `Simpsons` is carried out in two stages. The first sets up the Booster optical parameters as functions of time (pass1). In the second stage, the ensemble of macro-particles is tracked through the fields of each element of the ring and space charge forces are calculated from the macro-particle distribution (pass2).

In addition to the input parameters there are more than ten time-dependent parameters details of which are fed in during the simulation runs. Each of the data files specifies how one or more physical parameters change as a function of time during the running-cycle. Examples of changing parameters include the following:

- $B\rho$ during energy ramping;
- Horizontal and vertical set-tunes;
- The primary and higher harmonic RF voltages and relative phases.

2.2 Physical Parameters used in the Simulations

The simulations are allied to real machine settings during the Booster operations. All physical parameters as represented as functions of time taken

either from operational settings or from run-time read-backs. Table 1 lists the most important physical parameters of the Booster used in the simulations.

Table 1: Physical parameters used in the simulation of proton beams in the AGS Booster.

Parameter	Injection	$G\gamma = 3$	$G\gamma = 4$	Extraction
$G\gamma$	2.175007	3.0	4.0	4.5
W [MeV]	200.0	631.753	1155.095	1416.766
cp [GeV]	0.644445	1.258819	1.871318	2.160058
E [GeV]	1.138272	1.570026	2.093367	2.355038
$B\rho$ [Tm]	2.149636	4.198969	6.242046	7.205178
β	0.566160	0.801783	0.893927	0.917207
γ	1.213158	1.673316	2.231088	2.509974
η	-0.6362	-0.3143	-0.1581	-0.1159
h	1	1	1	1
hf [MHz]	0.841167	1.191240	1.328143	1.362779
R [m]	$201.78/2\pi$	$201.78/2\pi$	$201.78/2\pi$	128.453/4

2.3 Numerical Parameters used in Simulations

The total number of particles in the AGS Booster proton beam is of the order of 10^{11}-10^{12}. It is not practical to track all these particles in the simulations even with the most modern computing facilities. Therefore, the beam is modeled by a much small number of macro-particles, each representing a certain number of real particles depending on the "weight" assignment.

The choice of a suitable number of macro-particles is a balance between maintaining computational accuracy and controlling the CPU running time. The process is carried out for coasting beams (without longitudinal substructure) and bunched beams (where the longitudinal substructure must be taken into account) separately. The number of macro-particles is chosen to be one that can safely represent the real beam while it is either unbunched or bunched.

To determine the minimum acceptable number of macro-particles for the modeling, we need to identify a criterion. We consider a number of macro-particles to be "suitable" if the simulation results are within 5% of convergent results produced with increasingly large numbers of macro-particles. It is found that convergence in measurable quantities is reached with about 20000 macro-particles in the coasting beam case, and 50000 for bunched beams. The comparison suggests that 5000 macro-particles is adequate to obtain a result which is within 5% of the convergent results. In order to obtain slightly higher accuracy 10000 macro-particles were used for all the simulations in this study.

Another important numerical parameter is the time step-size during the tracking. In a similar way, a "suitable" integration step-size can be identified by considering the convergence of results as the time step is made smaller and smaller. A time step is considered "suitable" if the results it produces are within 5% of the convergent results. Convergence is certainly reached with step 0.1 nsec. The analysis concludes that a time step of 10 nsec can be realistically used to obtain a result which is within 5% of the convergent results in a reasonable CPU time. Therefore, 10 nsec was used as the time step-size for all the simulations in this study.

The details of numerical parameter determinations by comparison of simulation results are presented in Subsection 4.2 in [2].

3 Physical Aperture and Beam Loss

3.1 Physical Aperture in the Booster

The physical apertures are taken to be the inside dimensions of the vacuum chamber around the Booster ring. The geometry of the vacuum chambers is circular, with exceptions where dipoles are located. Figure 1 illustrates the top view and cross-section of the Booster dipole vacuum chamber taken from Figure 6-2 of the "Booster Design Manual" [4]. This cross-section is implemented in the simulations as an elliptical shape with the same dimensions as

shown in Figure 1. The dimensions of the vacuum chamber at each element around the Booster ring are listed in Table 2.

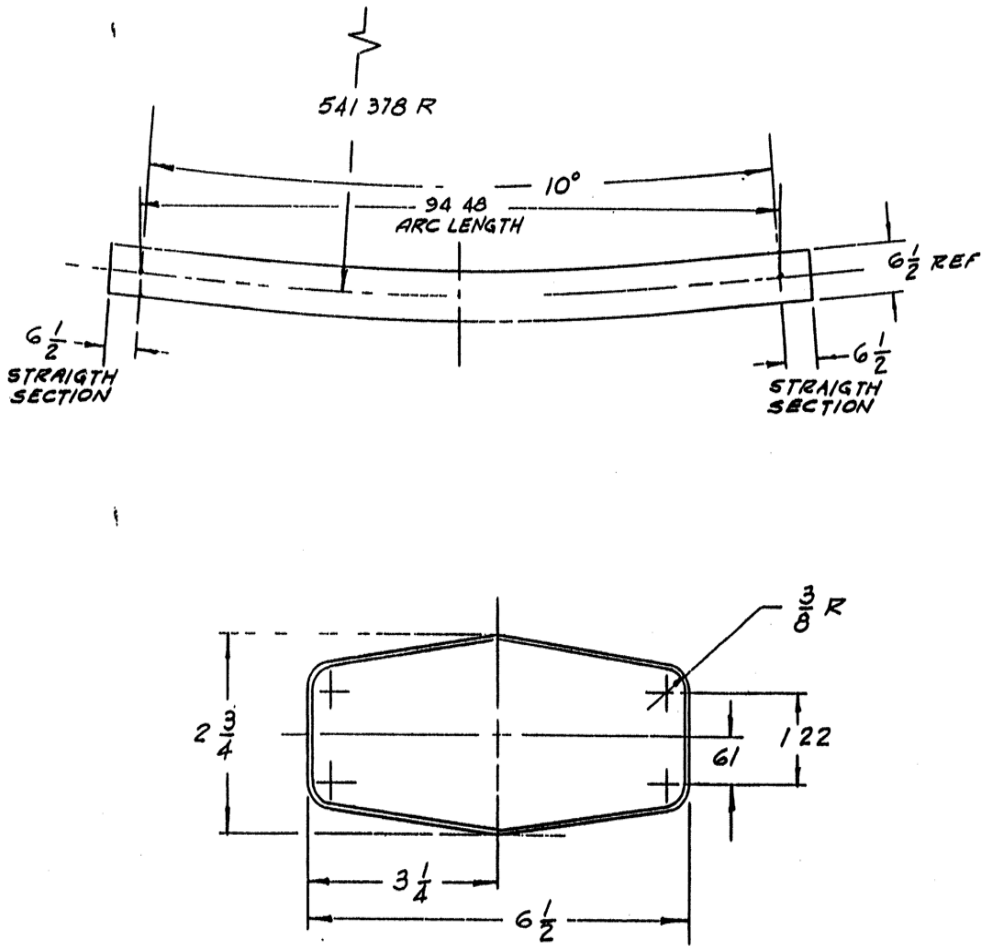

Figure 1: The top view and cross-section of the Booster dipole vacuum chamber.

Table 2: Physical aperture implemented in the simulations of proton beams in the AGS Booster.

Elements	Keyword	Num.	Length [m]	Shape	Apert. R[mm]	% of Ring
Dipoles	DH	36	2.42	elliptic	82×34	43.18
Quadrupoles	QH	24	0.493	circular	66	5.86
Quadrupoles	QV	24	0.504	circular	66	5.99
Sextupoles	SH, SV	48	0.1	circular	82	2.38
Drift (at Kicker)	L057	43	0.5704			12.16
Drift (at PUE)	L014	48	0.1381	circular	76	3.28
Drift (at PUE)	L012	24	0.1173	circular	76	1.4
Drift (at PUE)	L011	24	0.1118	circular	76	1.33
Drift (at Septum)	(COD)				47×33	
Drift	L007	48	0.0696	circular	76	1.66
Drift	L2757	1	2.7569	circular	76	1.37
Drift	LDH	6	2.42	circular	76	7.2
Drift	LDHH	6	1.21	circular	76	3.6
Drift	LDH1	1	1.5	circular	76	0.7
Drift	LDH2	1	0.32	circular	76	0.16
Drift	LDH3	1	0.32	circular	76	0.16
Drift	LDH4	1	0.28	circular	76	0.14
Drift	L032	1	0.3058	circular	76	0.15
Drift	L031	24	0.2954	circular	76	3.51
Drift	L030	3	0.2937	circular	76	4.37
Drift	L029	23	0.2899	circular	76	3.3
Drift	L028	5	0.2767	circular	76	6.86
Drift	L0218	1	0.2176	circular	76	0.11

3.2 Impact of Physical Aperture on Beams

In general, there are many causes of beam loss, including: H^- ions missing the foil; foil scattering; imperfect charge exchange; unoptimized injection parameters; longitudinal beam halo, perhaps related to imperfect beam chopping leading to uncaptured beam; unoptimized RF program that allows beam to leak out of the bucket into unstable regions of phase space; transition crossing; extraction issues. Some of these are not issues in the AGS Booster, and they may be attributed to the basic machine design. Study of others, such as beam loss due to effects of foil scattering, is presented in other reports (such as in Sections 5.1 and 5.2 in [2]).

This part of the study is to investigate the impact of physical aperture on the AGS Booster beams at each stage of the cycle. Here, "beam loss" is defined as follows: Whatever the reasons, a macro-particle circulating in the Booster with a large transverse excursion from the center of a vacuum chamber, is considered to be completely lost from the circulating beam when it reaches the machine physical aperture. Macro-particles whose longitudinal excursion goes beyond half the RF bucket length are considered as "potentially lost" since they are then in an unstable region of phase space, but they are retained in the simulation, and their presence still has an effect on the space charge in the circulating beam, until such time as their enhanced momentum, combined with dispersion, causes them to be physically lost at the machine physical apertures.

In order to quantitatively describe the beam loss in a Booster cycle, in this study, a "beam loss parameter" is introduced and is defined as the fraction of accumulated beam loss to the total beam in the ring when injection completes. It is calculated as a function of time counting from the start of Booster injection (time = 0 msec). The bottom graph in Figure 2 is an example of beam loss parameters.

In order to explore the impact of physical aperture on the beams, we performed six sets of simulations with six different physical apertures. One simulation is with the realistic physical aperture as listed in Table 2. The other five simulations are performed as comparison cases with unreal physical apertures that differ from the realistic Booster apertures listed in Table 2. In

this comparison study, the injected beam, charge exchange foil, the Booster lattice, energy ramping, and RF settings are kept the same for all six cases. The only differences are in their physical apertures.

In the five comparison cases, the physical apertures at dipoles, quadrupoles and sextupoles are kept to be the same as in the realistic case (which is 57.4% of the whole Booster ring), but the physical apertures at other locations (42.6% of the Booster ring) are set to be either smaller or larger than the real Booster apertures.

Of the comparison cases, those with $R_{\rm drift}$ =34 mm, 47 mm and 66 mm have smaller values than real Booster physical apertures of $R_{\rm drift} = 76$ mm. These three cases correspond to assuming the drift tube apertures at non-magnet locations are as small as the apertures of vertical-in-dipoles, at beam-dump, and at quadrupoles, respectively. The other two comparison cases are with $R_{\rm drift} = 82$ mm and 200 mm, which are larger than the realistic Booster physical apertures of $R_{\rm drift} = 76$ mm. These two cases correspond to assuming the drift tube apertures at non-magnet locations are as large as the apertures at sextupoles and "no-limitation" (implemented by $R_{\rm drift}$ =200 mm), respectively.

The evolutions of bunching factor, longitudinal emittance and beam loss, as functions of time, are shown in Figure 2, and the horizontal and vertical emittances are shown in Figure 3, respectively. The red curves ($R_{\rm drift} = 76$ mm) show the simulation results with the realistic physical aperture as listed in Table 2. The other five cases ($R_{\rm drift}$ =34, 47, 66, 82 and 200 mm) are shown by blue, magenta, green, brown and purple curves, respectively.

By comparing these six cases, it may be coincluded that if physical aperture is too small ($R_{\rm drift} < 66$ mm) the beam emittance and beam loss rate are significantly impacted by the physical aperture. Otherwise, in the cases of $R_{\rm drift} >$ 66 mm, the physical apertures do not have much impact on the beams. Therefore, in general, the realistic physical aperture in the Booster ($R_{\rm drift}$ =76 mm) can accommodate the operations with higher intensity beams.

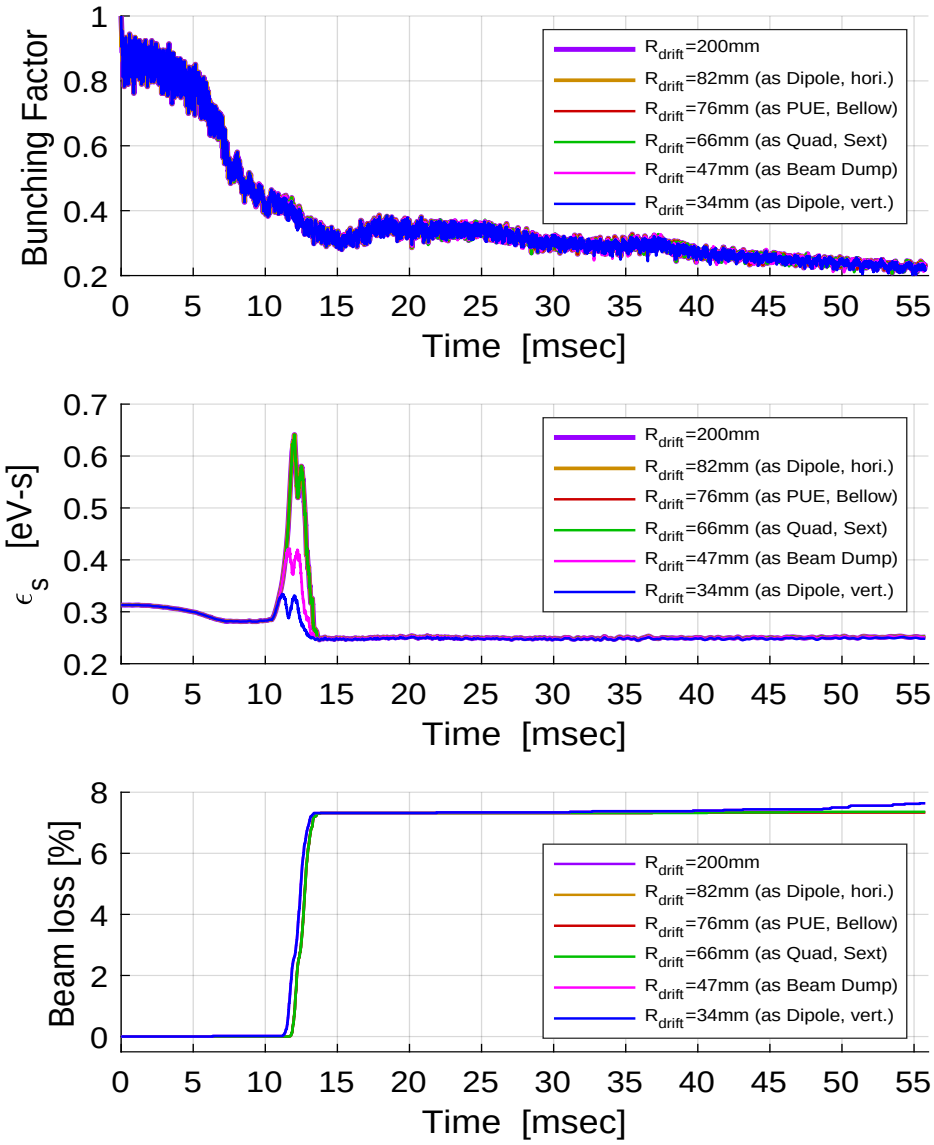

Figure 2: Bunching factor, longitudinal emittance and beam loss as functions of time. The realistic case ($R_{\rm drift}$ = 76 mm) is shown by the red curve. The other five comparison cases ($R_{\rm drift}$ =34, 47, 66, 82 and 200 mm) are shown by blue, magenta, green, brown and purple curves, respectively.

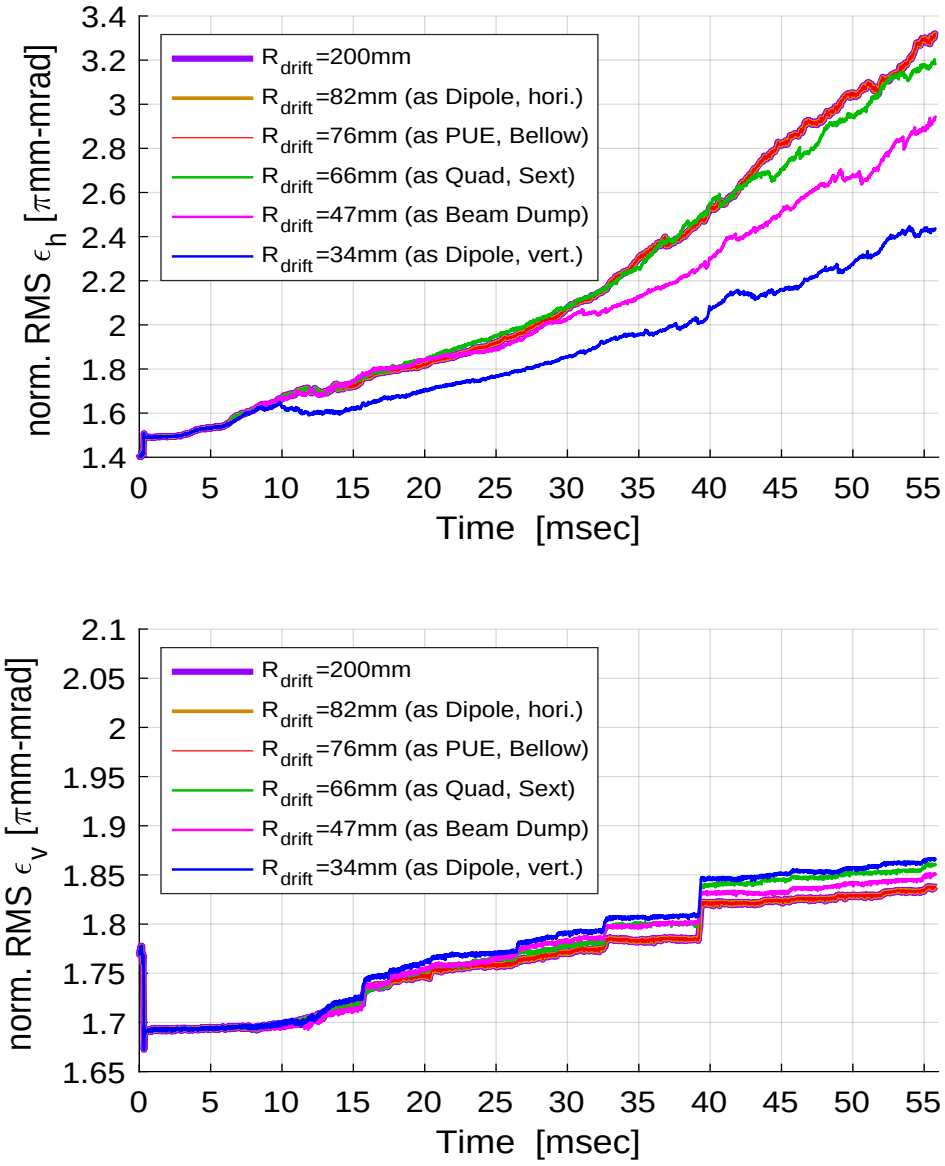

Figure 3: Horizontal and vertical emittances as functions of time. The realistic case ($R_{\rm drift}$ = 76 mm) is shown as a red curve. The other five comparison cases ($R_{\rm drift}$ =34, 47, 66, 82 and 200 mm) are shown by blue, magenta, green, brown and purple curves, respectively.

4 Injection

To achieve the goal of increasing the beam intensity in polarized protons injected into the Booster, we could either extend the injection pulse length or increase the intensity of the polarized H^- ion beam by increasing the Rb cell temperatures in OPPIS (Optically Pumped Polarized H^- Ion Source) [5]. In this section, we investigate the impacts of higher intensity of injected beam, longer injection pulse length, different charge exchange foil thickness and the related space charge effect during the Booster injection process.

4.1 Impact of Higher Intensity of Injected Beam

The polarized proton beam is converted from polarized H^- ions produced in OPPIS [5]. In general, during OPPIS operations, a higher output beam intensity requires a higher Rb cell temperature. As a result of increased Rb cell temperature, the emittance of the polarized H^- ion beam is increased, thereby increasing the emittance of converted polarized proton beam through charge exchange foil.

Data from measurements in the Booster taken by Keith Zeno [6] were used to establish the relationship between the emittance and the intensity of the polarized proton beams injected into the Booster and the Rb cell temperatures in OPPIS. Figure 4 shows the current-transformer during the measurements. The top yellow trace is a higher input case and the bottom yellow trace is a lower input case. The pink trace is with higher input but without Booster optimization for that input. The red trace is the dual harmonic (B3) voltage. The first beam loss at $\sim$110 ms is due to horizontal scrape. The second beam loss at $\sim$130 ms is due to vertical scrape. The intensity measurements are performed at "Booster injection" and at "Booster late" which is after horizontal and vertical scrapes, but before Booster extraction. The injection pulse length was the same (300 μsec) for both cases. The settings for the amount of beam scraping are also kept the same for both cases. So, the measurement data, listed in Table 3, can be used to establish the relationship between the emittance and the intensity of polarized proton beams injected into the Booster due to the Rb cell temperatures in OPPIS.

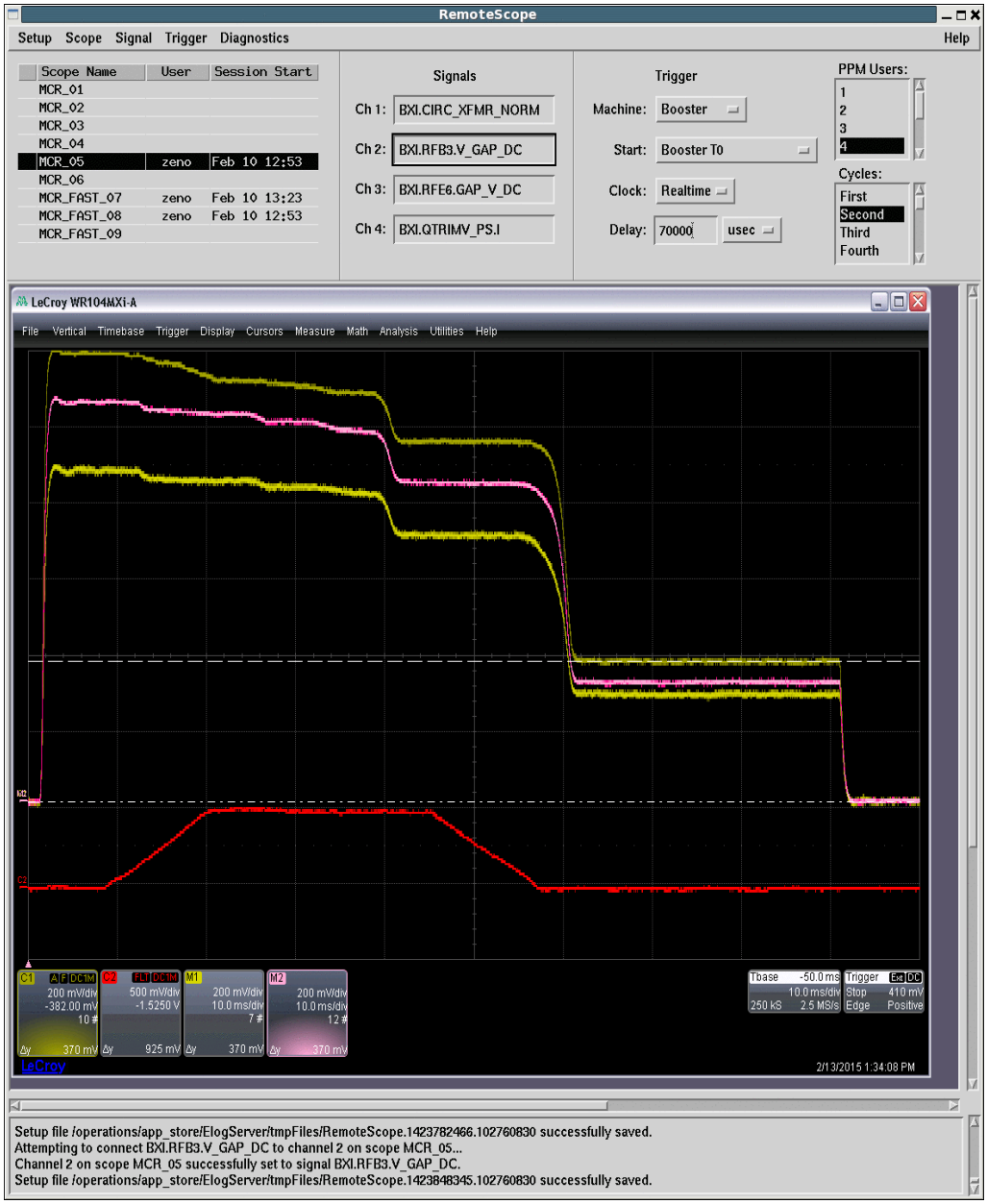

Figure 4: The current-transformer during the measurements. The yellow traces, top and bottom, correspond to higher/lower input espectively. The pink trace is with higher input but without any corresponding Booster optimization. The red trace is the dual harmonic (B3) voltage.

Table 3: The measurement data used to establish the relationship between the emittance and the intensity of polarized proton beams injected into the Booster due to the Rb cell temperatures in OPPIS.

Booster Input case	OPPIS Rb cell temperature	protons @ Injection	protons @ "Booster late"
Higher intensity	95°	14.5×10^{11}	3.7×10^{11}
Lower intensity	83.5°	8.7×10^{11}	2.82×10^{11}

Figure 5 shows the measured data (dark blue) and the extrapolations into the unmeasured regions by polynomial fits. The red, cyan, green and magenta curves show Rb cell temperature, "Booster Late", the ratio of Booster Later to "Booster Injection" and "emittance scale factor" as function of Booster Injection intensity, respectively.

4.2 Impact of Longer Pulse Lengths on the Injected Beam

As indicated at the beginning of this section, another way to achieve the goal of increasing the beam intensity is to extend the injection pulse length. However, the longer the pulse length, the higher the number of beam traversals through the charge exchange injection foil and the greater the proton beam emittance growth due to multiple scattering.

Figures 6 and 7 show the RMS and full (95%) emittances in the polarized proton beam injected into the Booster using a foil with thickness $100\,\mu g/cm^2$. The curves in blue, green, red, cyan and magenta correspond to injection pulse lengths of 200, 250, 300, 350 and 400 μsec respectively.

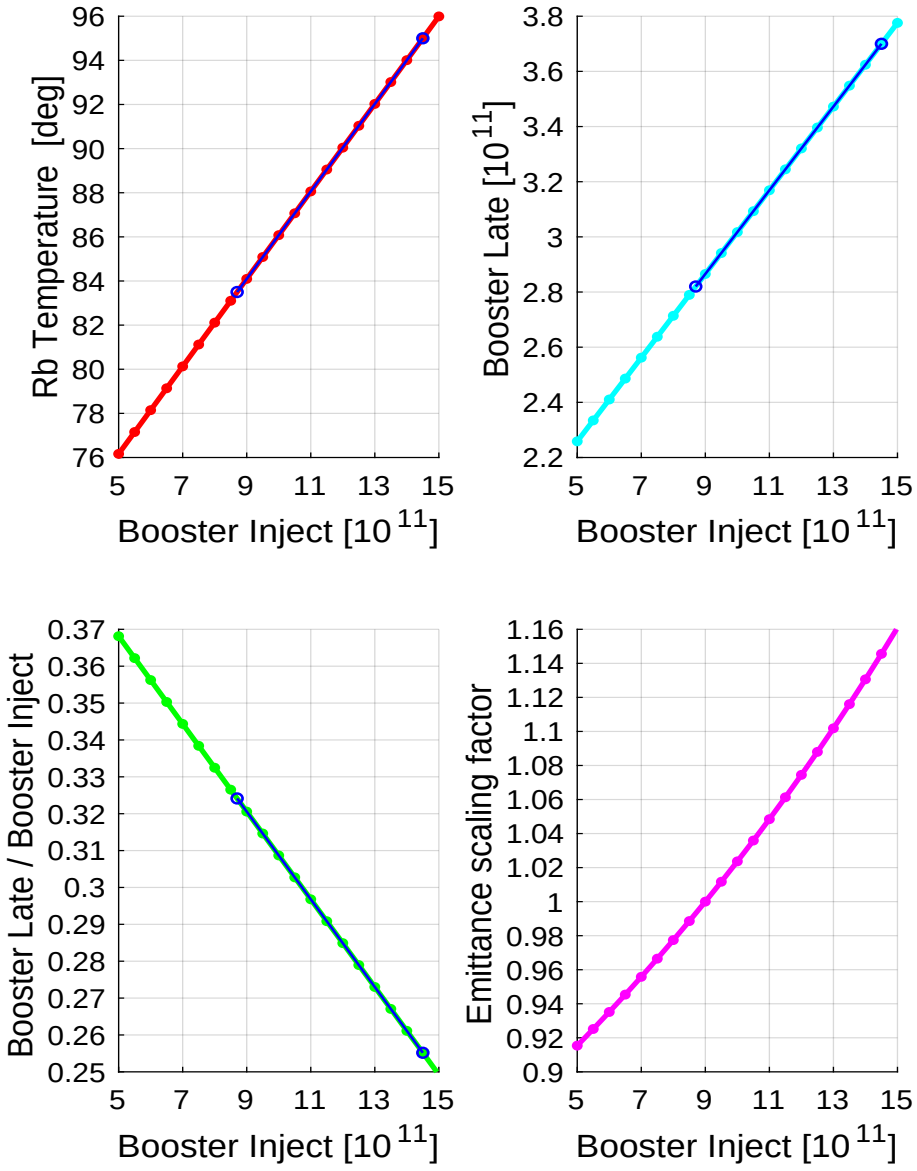

Figure 5: The measured data (dark blue) and the extrapolations into the unmeasured regions by polynomial fits. The red, cyan, green and magenta curves show Rb temperature, Booster Late, the ratio of Booster Later to Booster Injection and "emittance scale factor" as function of Booster Injection intensity, respectively.

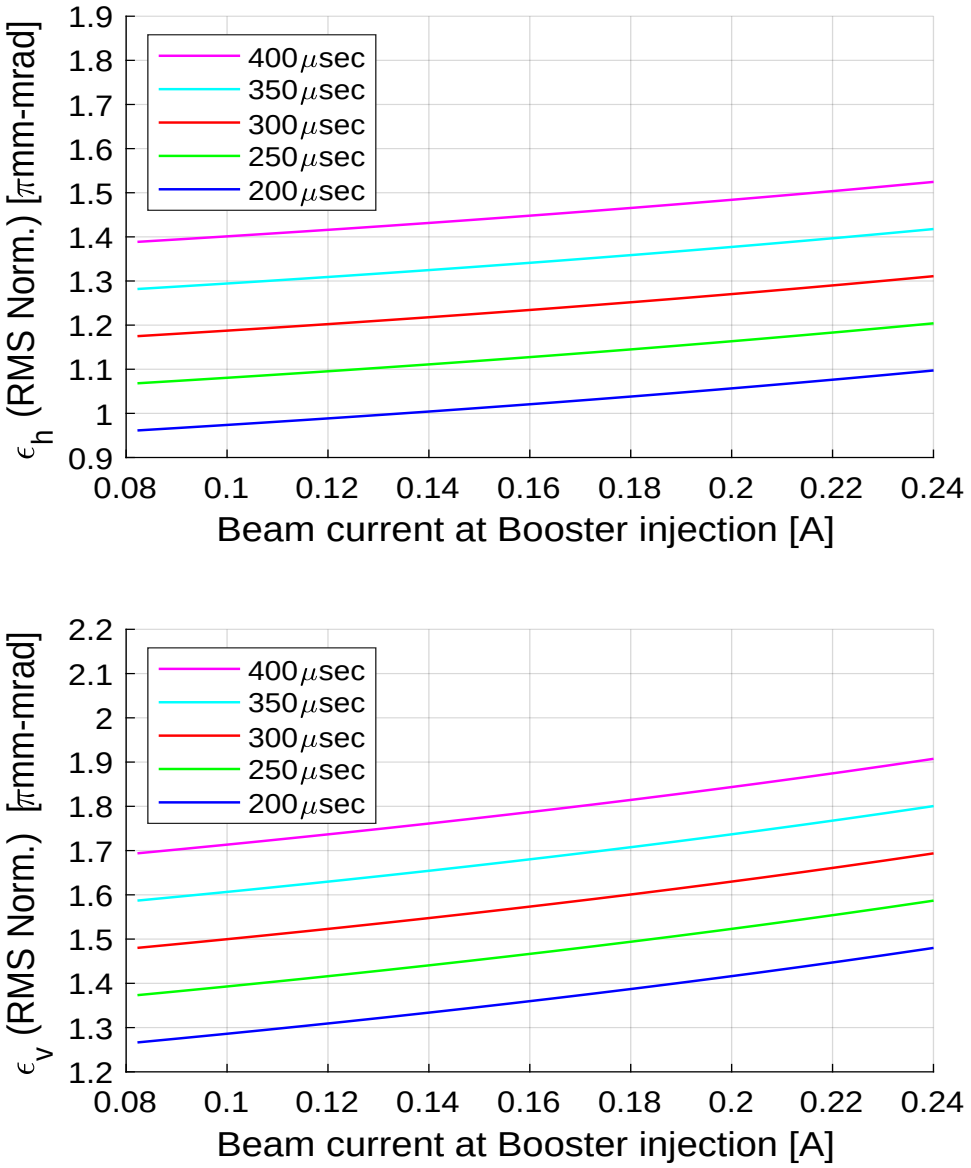

Figure 6: RMS emittance in the injected beams in horizontal and vertical phase space for five different injection pulse lengths with a charge exchange foil of thickness 100 μg/cm^2. The curves in blue, green, red, cyan and magenta correspond to injection pulse lengths of 200, 250, 300, 350 and 400 μsec respectively.

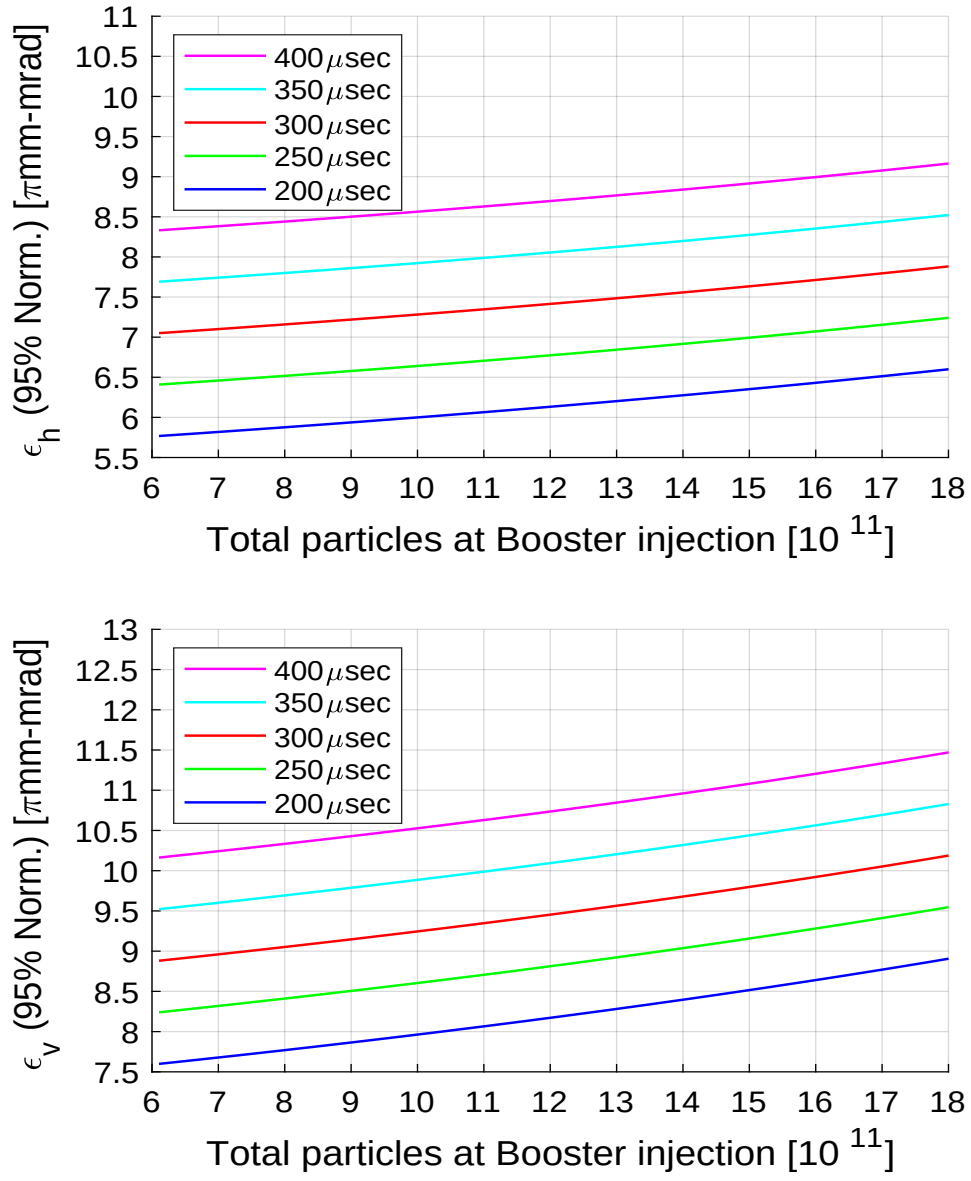

Figure 7: Full (95%) emittance in the injected beams in horizontal and vertical directions of five different injection pulse lengths through a charge exchange foil with thickness of $100\,\mu g/cm^2$. The curves in blue, green, red, cyan and magenta correspond to injection pulse lengths of 200, 250, 300, 350 and 400 μsec respectively.

4.3 Impact of Charge Exchange Foil Thickness

There are different kinds of charge exchange foils with different thicknesses available for injecting polarized protons into the Booster. (See Section 5.2 in [2] for details). The most common designs are "stamp" style and "strip" style. The available thicknesses are 75, 100, 135 and 200 μg/cm^2.

In this subsection we consider the impact of charge exchange foil thickness on the emittance of injected polarized proton beams. For the same H^- incident beam there are different relative yields of H^+, H^0 and H^- for different foil thicknesses, with correspondingly different degrees of beam loss and transverse emittance growth in the circulating proton beams.

Figure 8 shows the horizontal and vertical emittances as functions of the injected beam intensity associated with eight different foil thicknesses. Four of the eight foil thicknesses are currently available for Booster injection operations. The other four are not yet available, and they are presented purely as a study. In this study, the injection pulse length is 300 μsec and the properties of the injection beams are kept same for all eight cases.

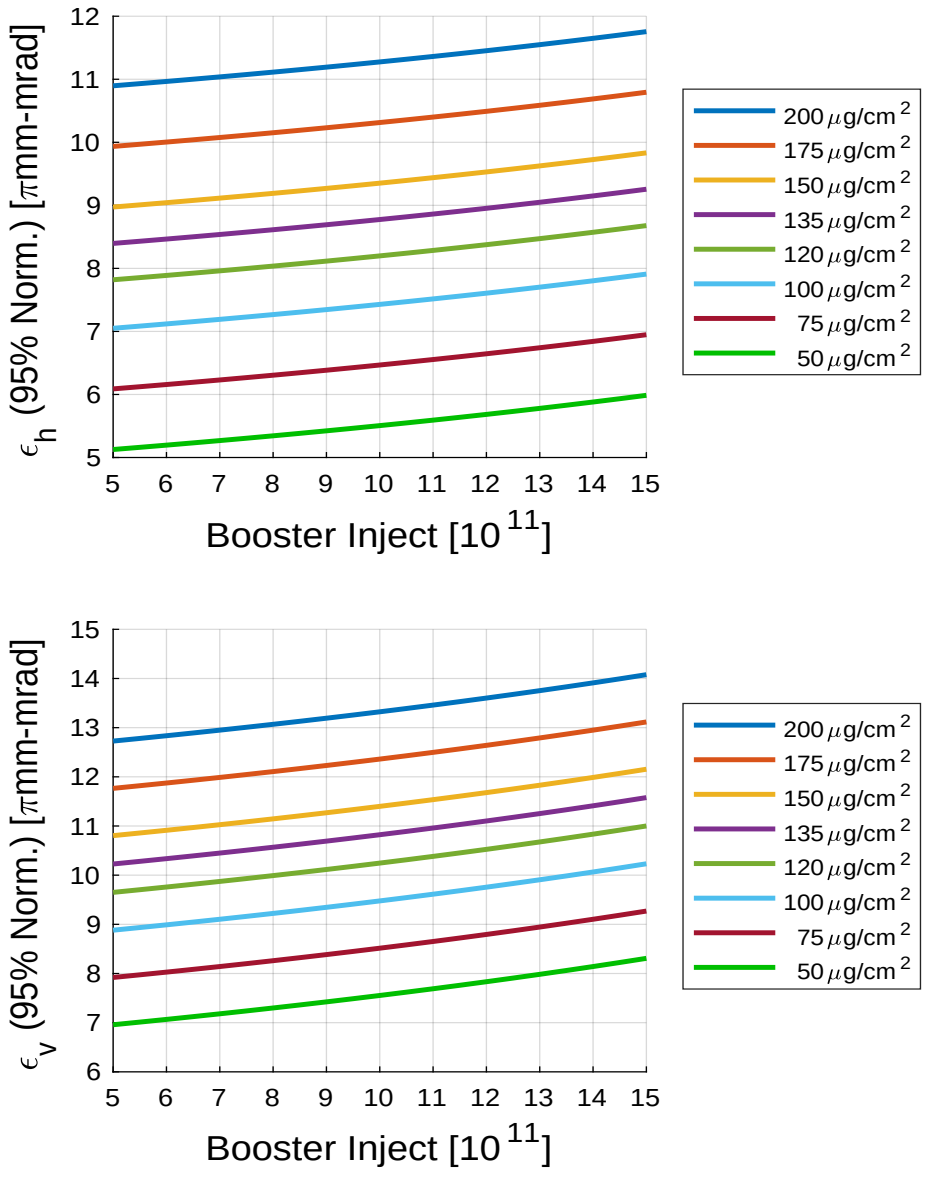

Figure 8: Horizontal and vertical emittances as functions of injected beam intensity for a range of foil thicknesses. The curvces correspond to a fixed injection pulse length of 300 μsec with all other beam properties unaltered.

4.4 Combined Effect of Injection Pulse Length and Foil Thickness

As discussed in Sections 4.2 and 4.3, for any given foil metrical, design and mounting mechanisms, the beam transverse emittance growth due to multiple scattering is related to the integral of the total time particles spend traversing the foil. For a given 4D transverse distribution, the longer the injection pulse, the more traversals the beam make through the foil during charge-exchange, and for a given proton energy, the thicker the foil, the more time a proton spends in each transit.

The quantitative data relating beam transverse emittance growth to foil thickness and pulse length have been measured in the AGS Booster by Keith Zeno [7]. Here, we extrapolate the measurement data to obtain the equal-emittance curves shown in Figure 9. Each data point on a curve represents the transverse emittance growth caused by a pair of parameters: "foil thickness [μg/cm^2]" and "injection pulse length [μsec]", with values marked on the abscissa and ordinate respectively.

Pairs of parameters on the same curve produce the same amount of transverse emittance growth via multiple scattering in the foil. For example, a data point on the red curve where the foil thickness is 100 μg/cm^2 and injection pulse length is 300 μsec represents the polarized proton operations of RHIC Run 2015. To increase the pulse length from 300 μsec to 400 μsec without additional transverse emittance growth, the foil thickness needs to be reduced to 75 μg/cm^2, corresponding to the top end of the red curve. On the other hand, if one changes the injection pulse length without changing the foil thickness one would face decreased/increased transverse emittance growth. Figure 9 makes it easier to estimate the combined effect of injection pulse length and foil thickness. It could also be a useful tool to aid decision-making on proton injection models.

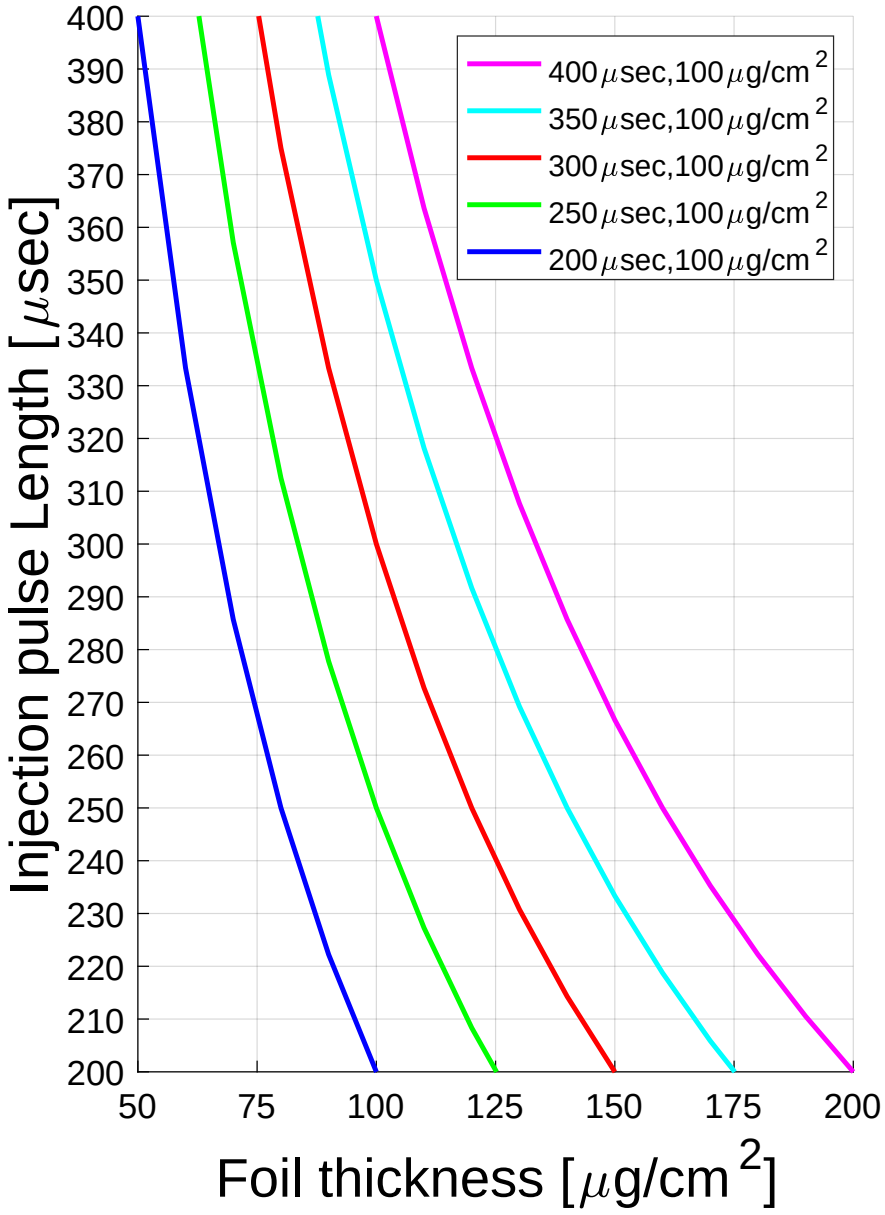

Figure 9: Equal-emittance curves extrapolated from the measurement data in the AGS Booster. Any pairs of parameters on the blue, green, red, cyan, magenta curve produce the same amount of transverse emittance growth as in the case via multiple scattering in the foil with thickness of 100 μg/cm^2 and with injection pulse length of 200, 250, 300, 350, 400 μsec, respectively.

4.5 Effect of Space Charge during Injection

The goal of this part of the study is to observe how a high intensity beam is affected by space charge by calculating the space charge tune shifts under Booster conditions during injection. As for actual Booster operations, the simulation model assumes the beam is injected into the Booster ring through a charge exchange foil and the desired intensity is accumulated over a period dictated by the chosen pulse length. In this part of the study we assume a foil thickness of $100\mu\text{g/cm}^2$ and an injection pulse length of $300\,\mu$sec. The accumulated 200 MeV coasting beam undergoes RF capture and acceleration, while the Booster tunes change from above half-integer to away from half-integer within the 4.3 msec immediately after multi-turn injection completes.

On this time scale, the beam evolves under the forces from the fast changing fields of the magnets, RF cavities and space charge effects. To observe beam evolution under this combined effect during injection and for the $200\,\mu$sec immediately after, we focus the study on single particle tracking and tune calculations.

In addition to tracking the total beam, a few test-particles are also tracked through the Booster cycle and their phase space coordinates x, x', y, y', pc, s and $\delta p/p$ are recorded at each turn and a one-turn transfer matrix constructed. Horizontal and vertical tunes are extracted from the transfer matrix at each turn. Considering the space charge effects are different for particles at the different locations in the beam, the simulations have been performed with six test macro-particles initially located at 0.5σ, 1σ, 1.5σ 2σ, 2.5σ and 3σ from the beam center.

Figure 10 and 11 show the horizontal and vertical tunes during Booster multi-turn injection in a normal intensity beam (7.5×10^{11} protons) and a high intensity beam (13×10^{11} protons), respectively. Comparing the tunes in Figure 10 to the operational tune-setting (black curve) one can conclude that at normal intensity, tune depressions due to space charge are about -0.07, -0.05, -0.04, -0.03, -0.02, -0.01 for each of the six macro-particles. Similarly, one can deduce from Figure 11 that the corresponding space charge tune depressions for the high intensity beam are about -0.11, -0.09, -0.06, -0.03, -0.02, -0.01.

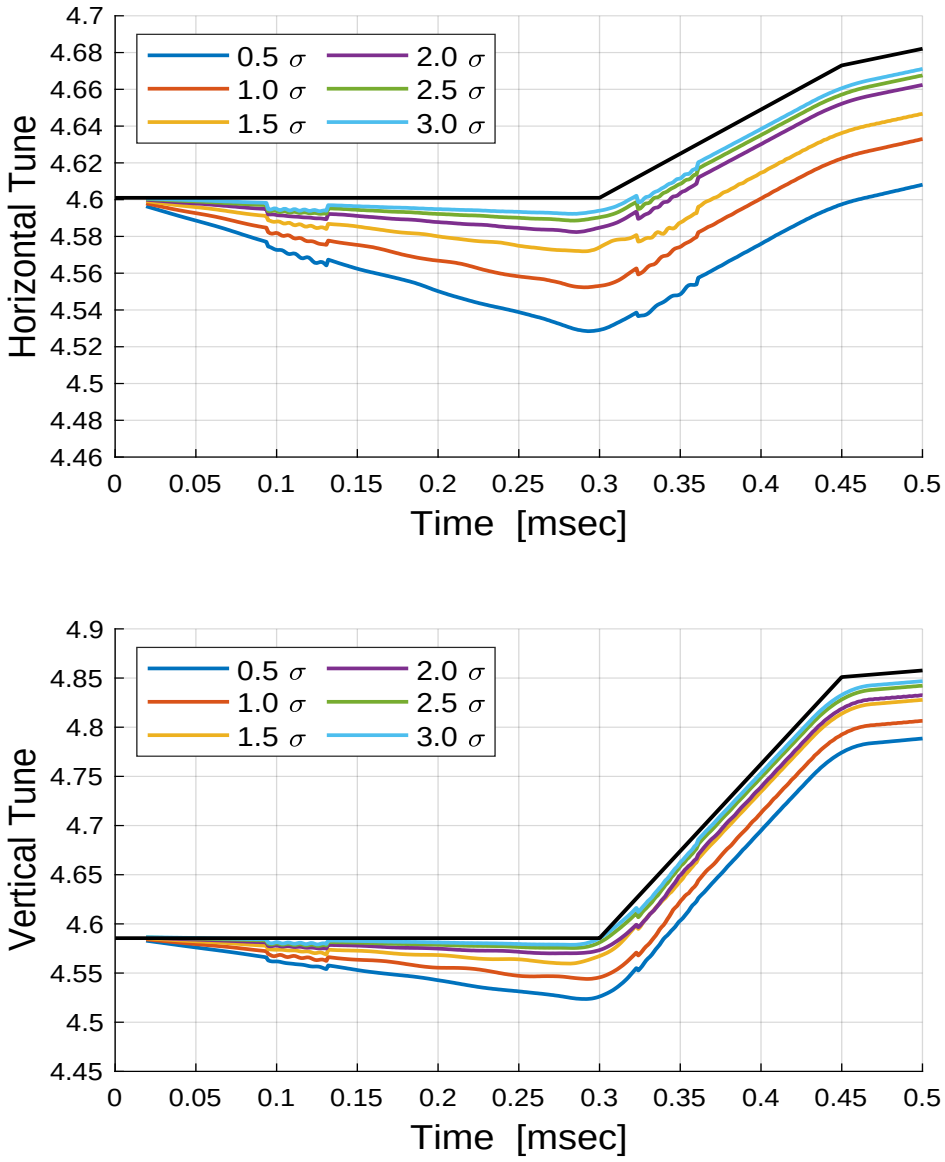

Figure 10: Horizontal and vertical tunes during normal intensity injection in which 7.5×10^{11} protons are injected into the Booster over a $300\,\mu$sec injection period.

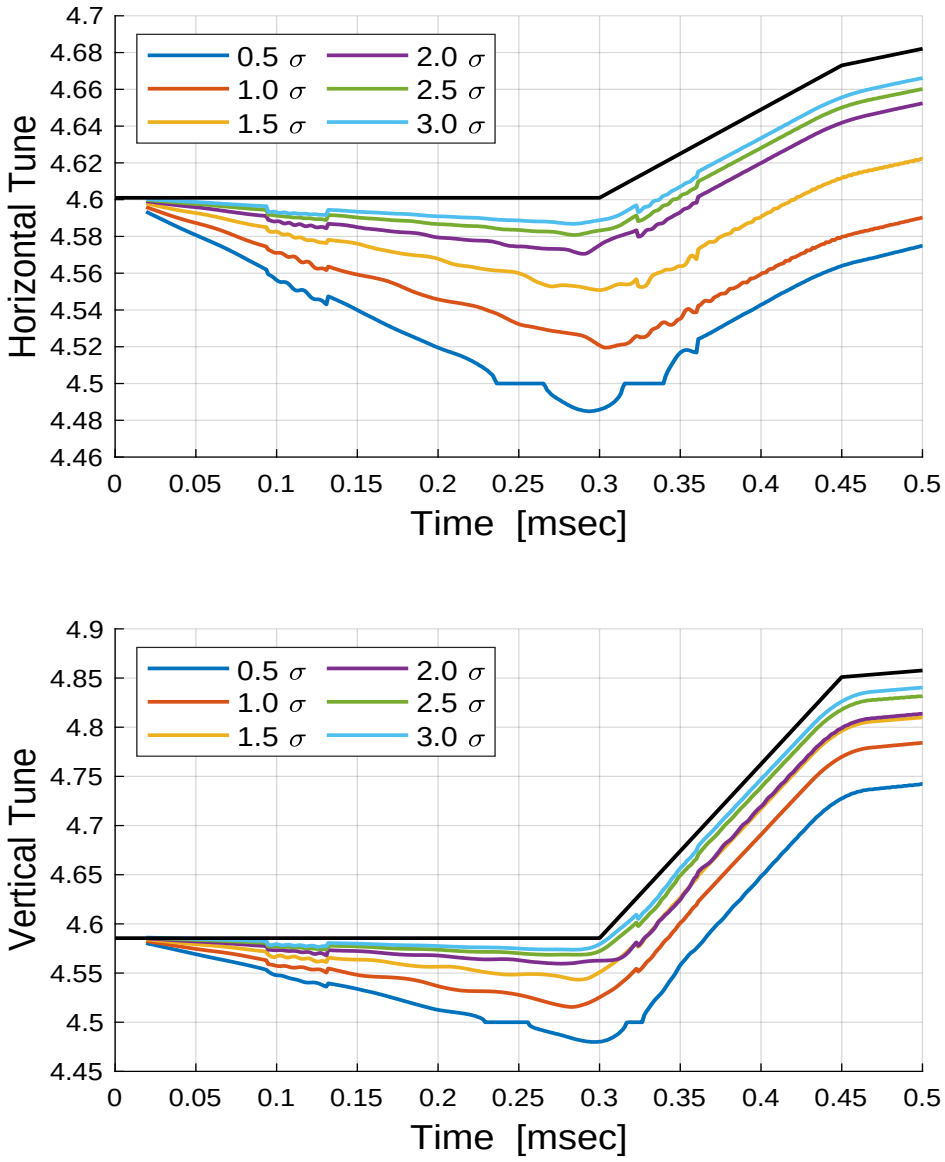

Figure 11: Horizontal and vertical tunes during a high intensity injection in which 13×10^{11} protons are injected into the Booster over a 300 μsec injection period.

Figure 12 shows the horizontal and vertical tunes developed at the end of multi-turn injection in beams of four different proton intensities at the end of 300 μsec multi-turn injection. Comparing the simulated tunes to the operational tune-setting (black curve), the tune depressions at intensities of 7.5×10^{11}, 9×10^{11}, 11×10^{11} and 13×10^{11} are seen to be about -0.05, -0.06, -0.08, -0.09 respectively.

5 Earlier Booster Cycle

During the earlier Booster cycle the injected beam evolves from coasting beam to bunched beam. Meanwhile, the beam is accelerated to a higher energy. Figure 13 shows the evolution of the particle distribution of a high intensity beam (13×10^{11}) in phase space during earlier Booster cycle. The purple, blue, green, yellow, brown and red dots represent the phase space distributions at the times (counting from beginning of injection) 1.2 msec, 7.2 msec, 8.4 msec, 9.6 msec, 11 msec and 12 msec, respectively. Since space charge effects are most significant when the particle energy is lower, in this section, we concentrate on the early stages of the Booster cycle.

5.1 Impact of Space Charge in the Early Stages of the Booster Cycle

Figure 14 and 15 show the horizontal and vertical tunes evolved during the early part of the Booster cycle in a normal intensity beam (7.5×10^{11} protons) and in a high intensity beam (13×10^{11} protons), respectively. The methods of test macro-particle tracking and tune calculation can be seen above, in §4.5.

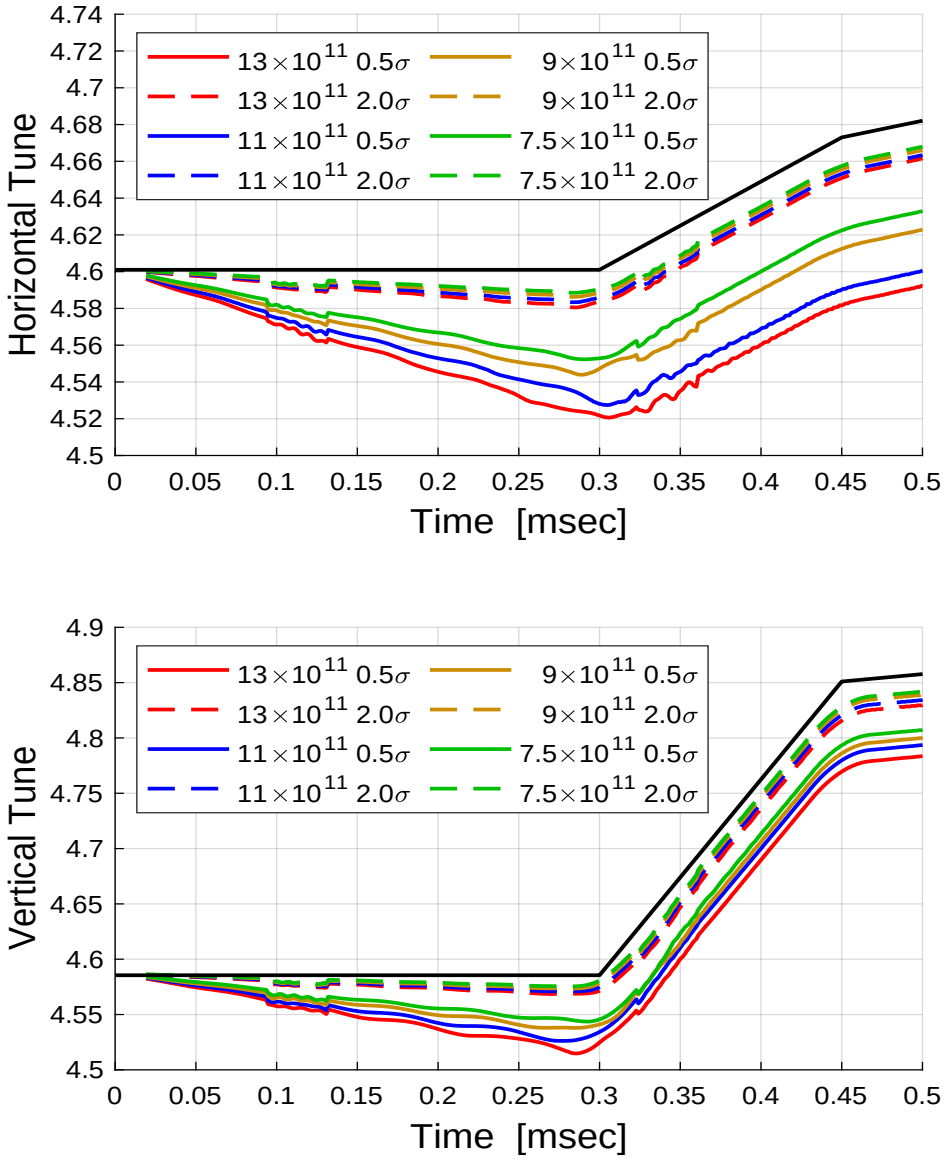

Figure 12: Horizontal tunes (upper sub-figure) and vertical tunes (lower sub-figure) developed in beams with four different intensities. The green, brown, blue and red curves correspond to proton beam intensities of 7.5×10^{11}, 9×10^{11}, 11×10^{11} and 13×10^{11} at the end of a 300 μsec multi-turn injection period. The black curve is the tune-setting during and after Booster injection.

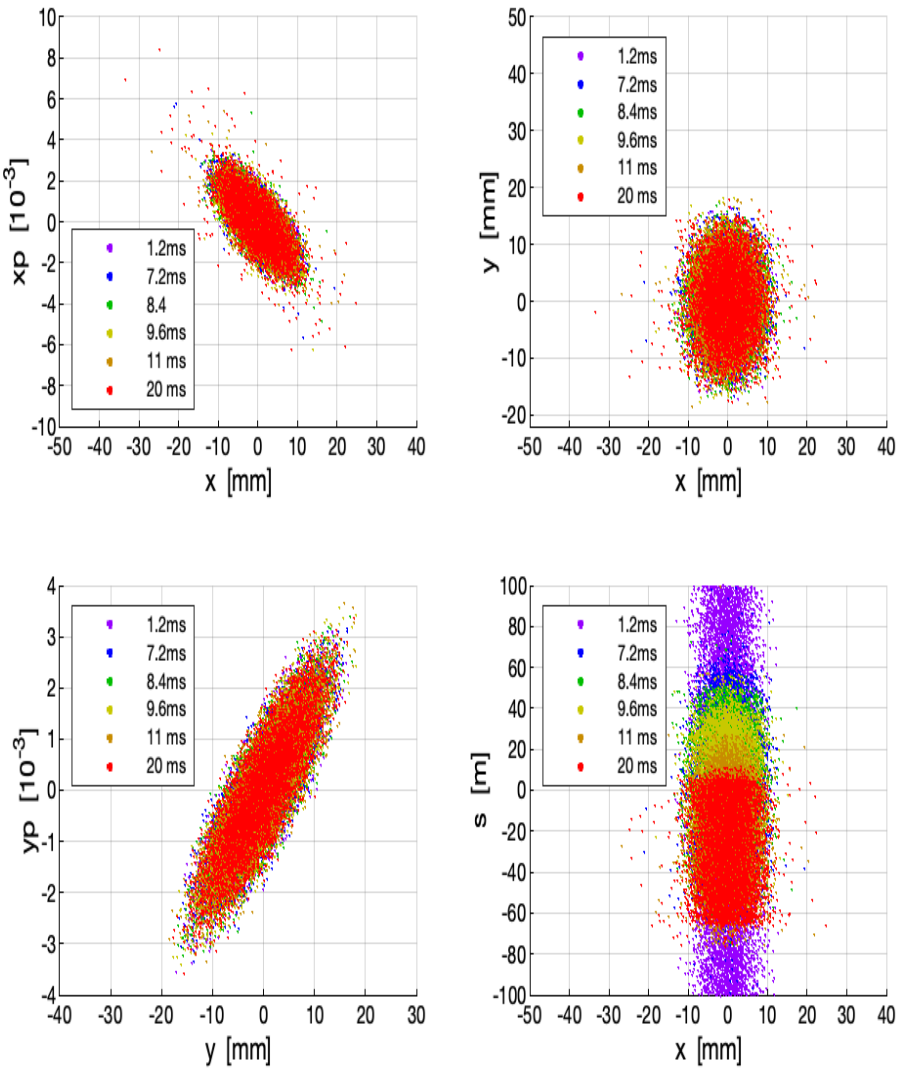

Figure 13: The evolution of the particle distribution of a high intensity beam (13×10^{11}) in phase space during earlier Booster cycle. The purple, blue, green, yellow, brown and red dots represent the phase space distributions at the times (counting from beginning of injection) 1.2 msec, 7.2 msec, 8.4 msec, 9.6 msec, 11 msec and 12 msec, respectively.

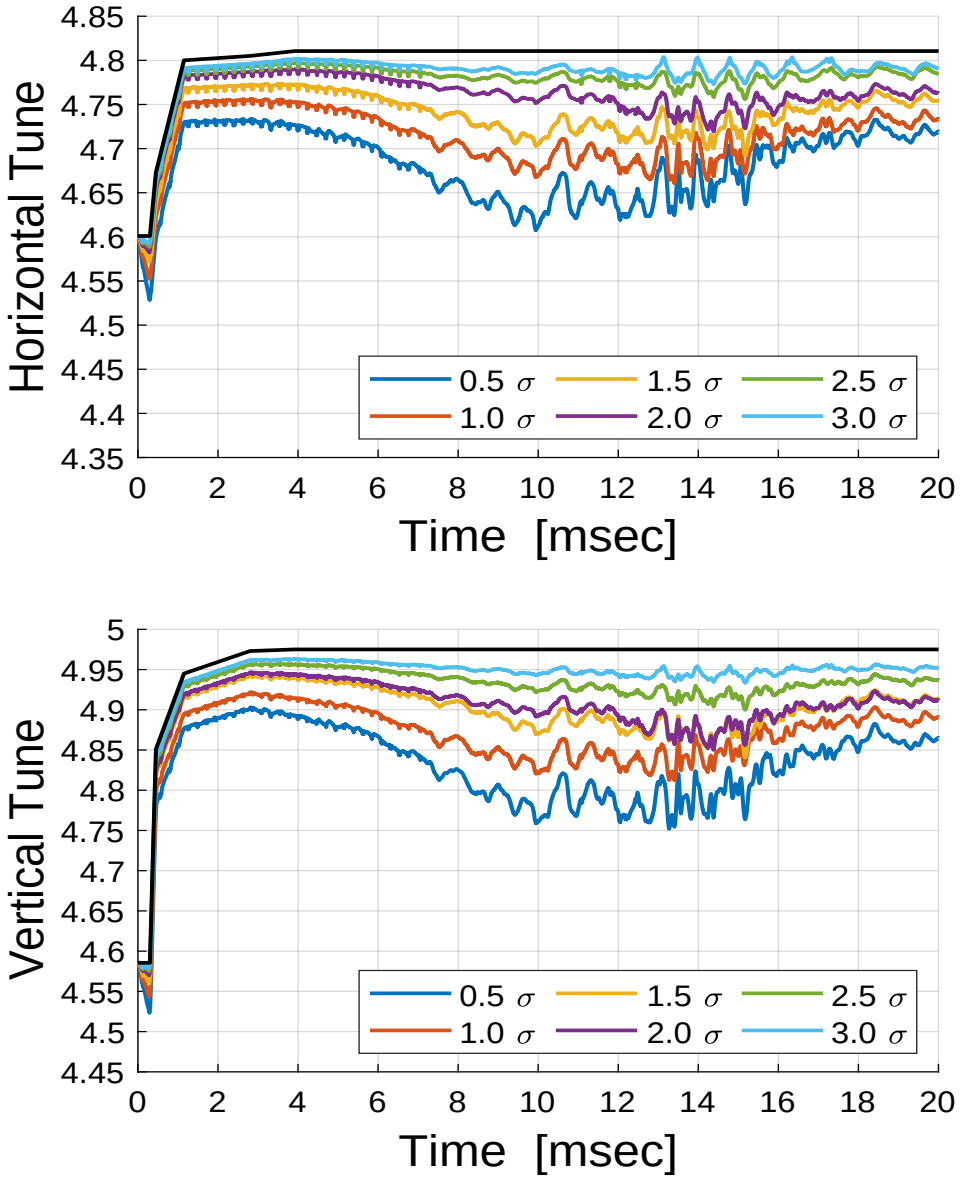

Figure 14: Horizontal and vertical tunes in a normal intensity beam (7.5×10^{11} protons) during the early part of the Booster cycle. The six colored curves are the tunes obtained from simulations of six test macro-particles initially located at 0.5σ, 1σ, 1.5σ 2σ, 2.5σ and 3σ from the beam center, respectively. The black curves are the set-tunes during the Booster operation.

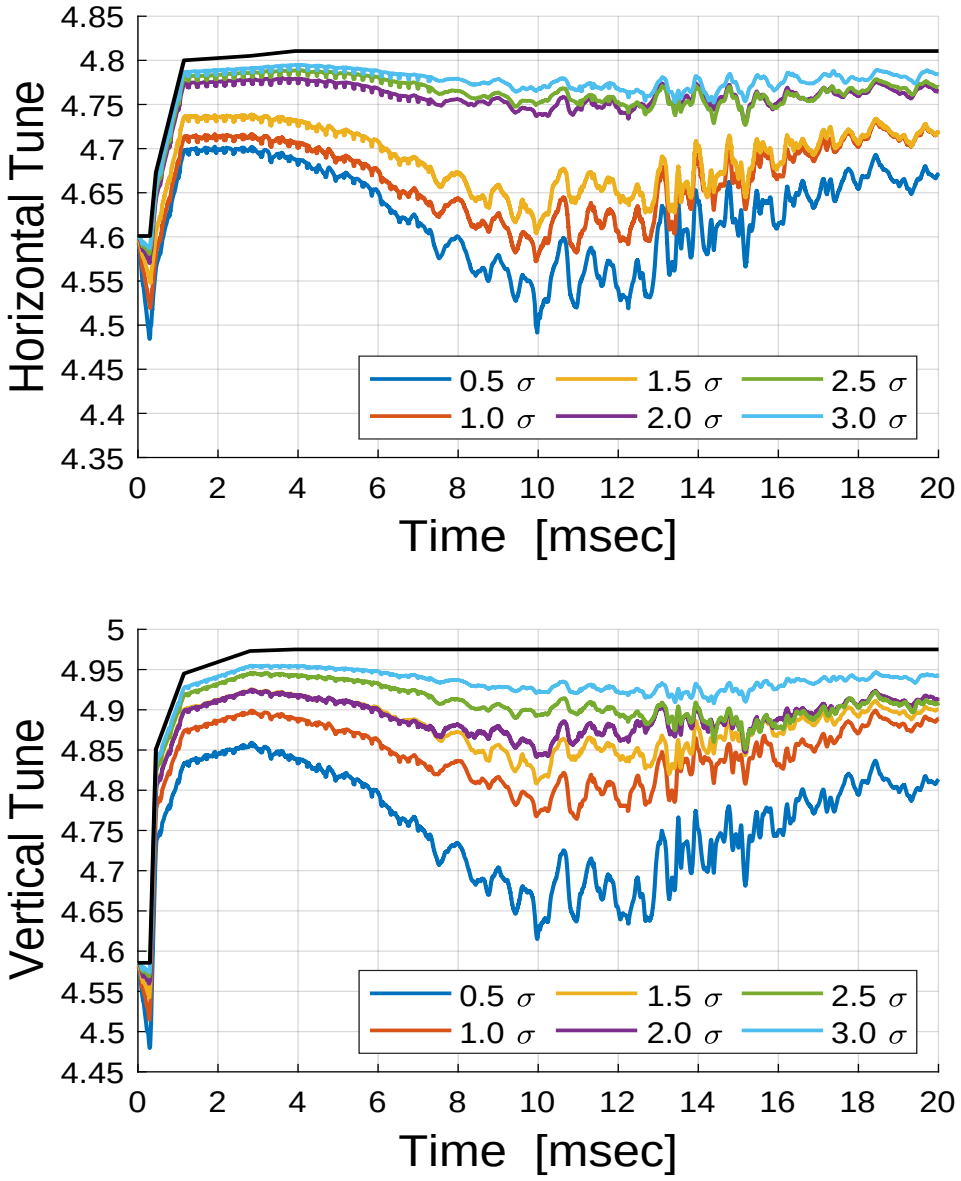

Figure 15: Horizontal and vertical tunes in a high intensity beam (13×10^{11} protons) during the early part of the Booster cycle. The six colored curves are the tunes obtained from simulations of six test macro-particles initially located at 0.5σ, 1σ, 1.5σ 2σ, 2.5σ and 3σ from the beam center, respectively. The black curves are the set-tunes during the Booster operation.

5.2 Impact of a Longer Pulse on the injected Beam

Figure 16 compares the transverse emittance evolution in normal intensity beams (7.5×10^{11} protons) that are injected into the Booster with three different pulse lengths (300μsec, 350μsec, and 400μsec). Since the space charge effect is not very significant at this intensity the transverse emittance grows at a similar rate in each case.

However, the situation is very different in high intensity beams. Figure 17 shows there is a much larger emittance growth in beams of 13×10^{11} protons injected with the same three different pulse lengths. The impact of a longer pulse of the injected beam and the associated initial emittances is no longer significant in the presence of stronger space charge effect in the high intensity beams.

Figure 18 illustrates comparisons of the horizontal and vertical tunes in high intensity beams during the early part of the Booster cycle. The red, blue and green curves are the tunes obtained from simulations of beams injected via a charge exchange foil of thickness is $100\,\mu\text{g/cm}^2$ with injection pulse lengths of 300μsec, 350μsec and 400μsec, respectively. The solid, dashed and dotted curves represent the tunes simulated with the test macro-particles initially located at 0.5σ, 1σ and 3σ from the beam center, respectively. The black curves are the set-tunes during the Booster operation.

The longitudinal beam properties are not significantly affected by the longer pulse lengths. Figure 19 shows a comparison of bunching factor, longitudinal emittance and beam loss in normal and high intensity beams (7.5 and 13×10^{11} protons). One can observe that longitudinal beam properties evolve in similar ways in all the cases. The beam loss rates may not be accurate due to the poor statistics when the beam loss rates are below 0.1%.

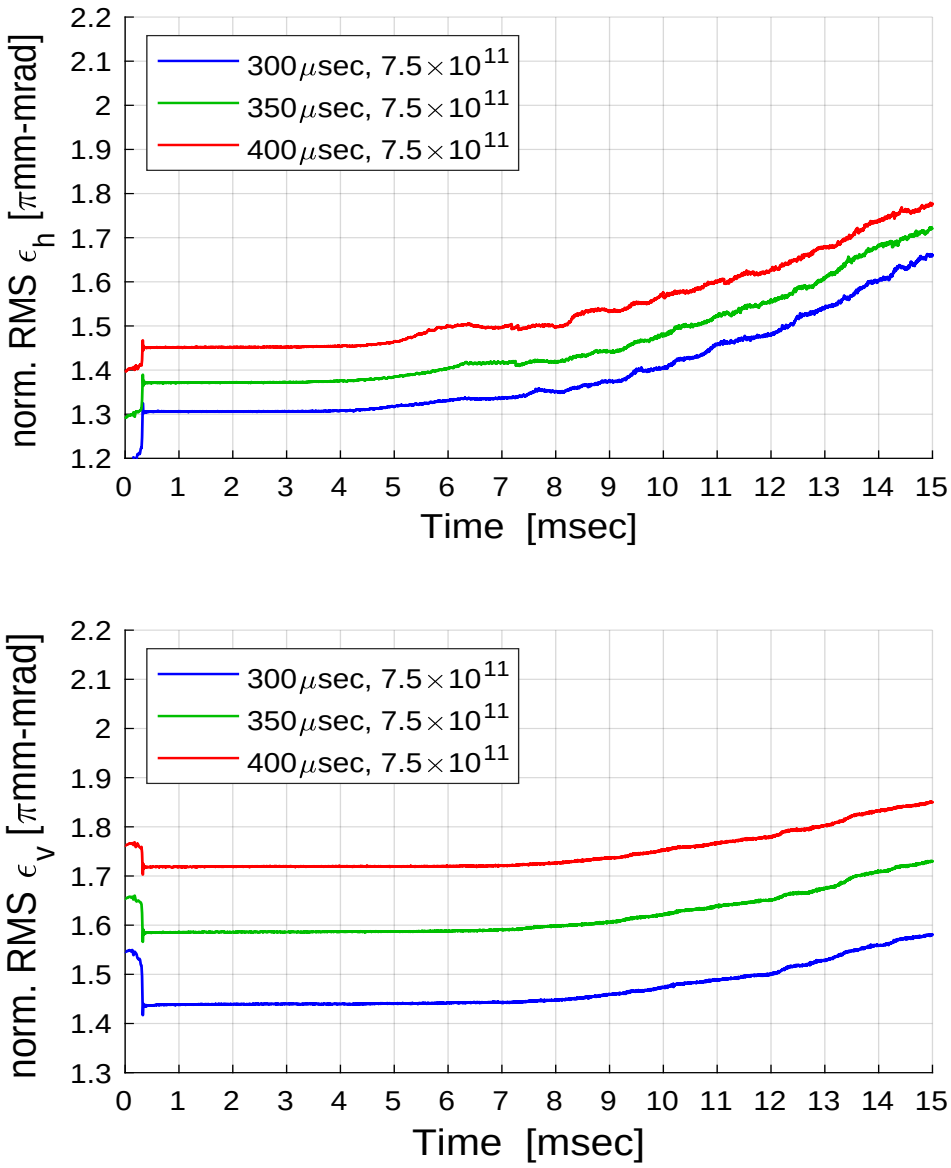

Figure 16: Horizontal and vertical emittance in a normal intensity beam (7.5×10^{11} protons).

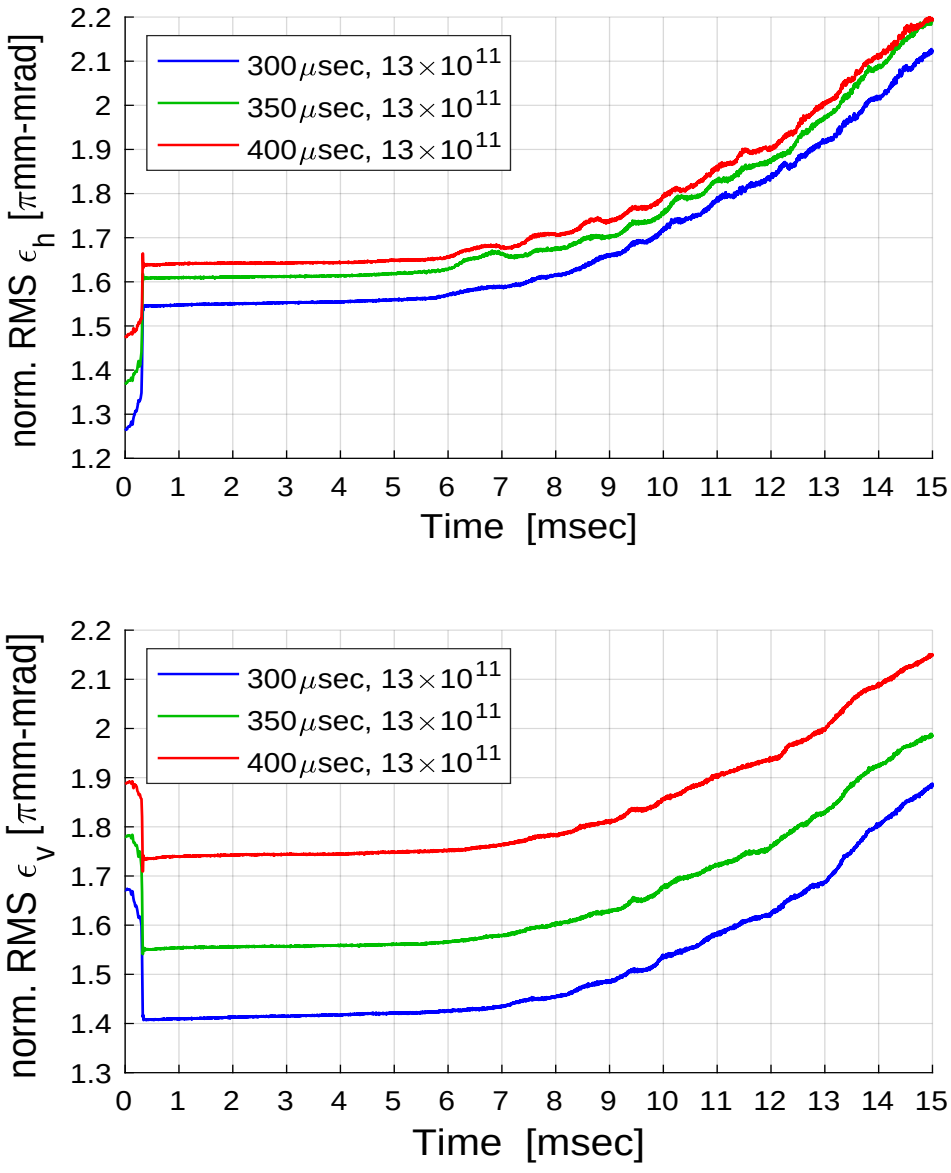

Figure 17: Horizontal and vertical emittance in a high intensity beam (13×10^{11} protons).

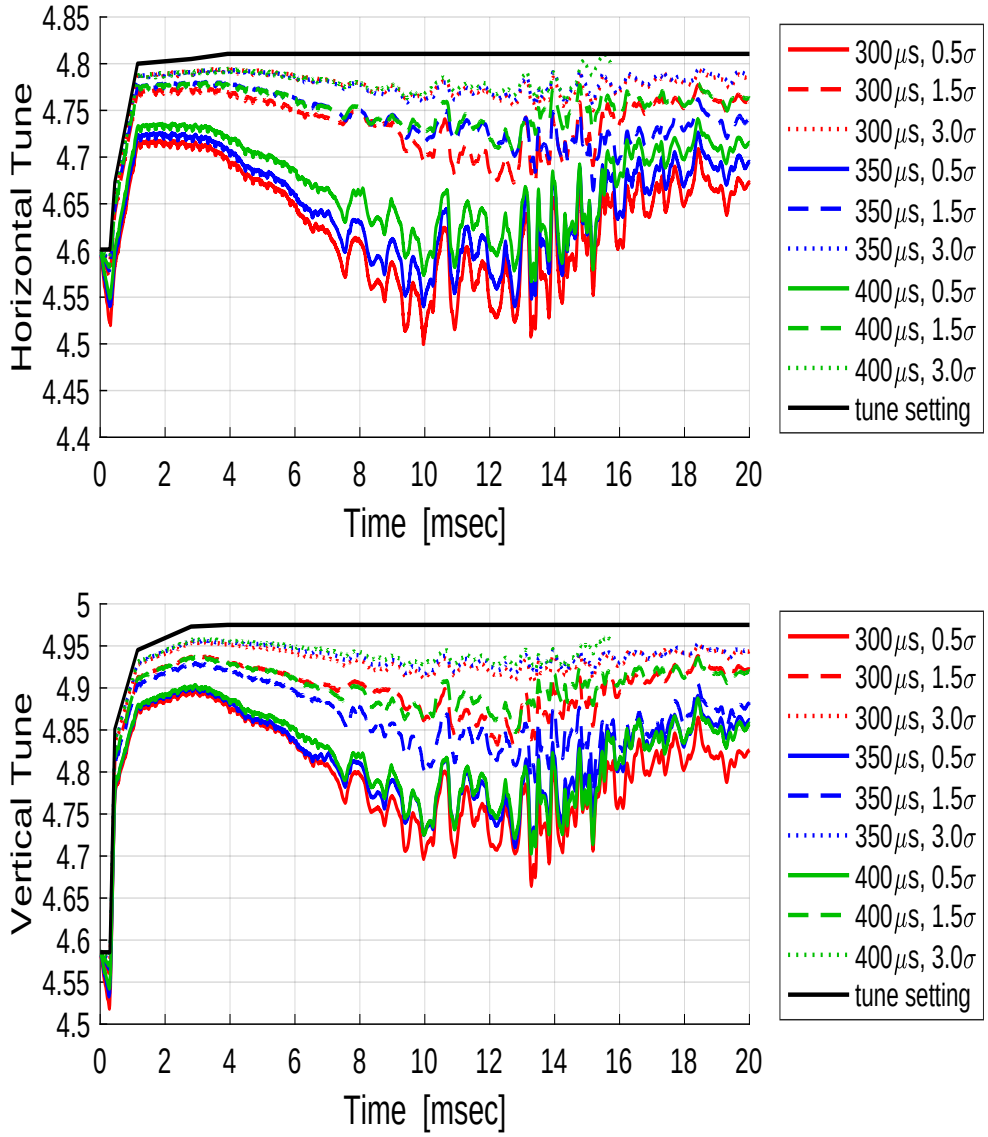

Figure 18: Comparisons of the horizontal and vertical tunes in a high intensity beam (13×10^{11} protons) during the early part of the Booster cycle. The red, blue and green curves are the tunes obtained from simulations of beams injected via a charge exchange foil of thickness is $100\,\mu g/cm^2$ with injection pulse lengths of 300μsec, 350μsec and 400μsec, respectively. The solid, dashed and dotted curves represent the tunes simulated by test macroparticles initially located at 0.5σ, 1σ and 3σ from the beam center, respectively. The black curves are the set-tunes during the Booster operation.

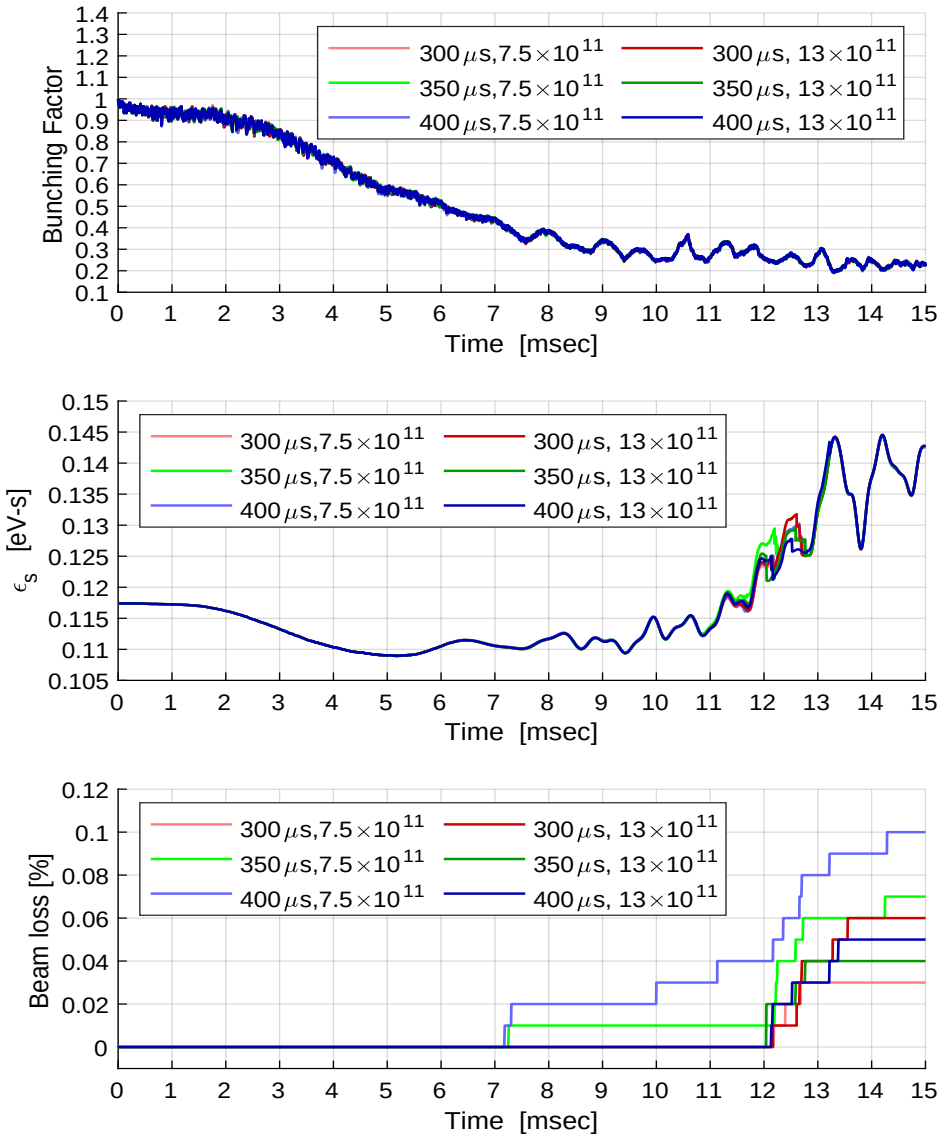

Figure 19: Bunching factor, longitudinal emittance and beam loss in a normal intensity beam (7.5×10^{11} protons) and a high intensity beam (13×10^{11} protons).

5.3 Impact of Higher Intensity of Injected beam

Emittance growth caused by space charge is more significant in high intensity beams than in beams with lower intensity. We consider specific beams with the four intensities 7.5×10^{11}, 9×10^{11}, 11×10^{11} and 13×10^{11} protons. Figure 20 shows the simulation results of transverse emittance evolution and Figure 21 demonstrates how the horizontal and vertical tunes evolve during the early part of the Booster cycle. The black curves are the set-tune during the booster operation.

5.4 Impact of Momentum Spread in the Injected Beam

Figure 22 compares the transverse emittance evolution in normal intensity beams (7.5×10^{11} protons) that are injected into the Booster with twelve different initial momentum spreads of (1, 1.5, 2, 2.5, 3, 3.5, 4, 4.5, 5, 5.5, 6, 7)$\times 10^{-4}$. Simulation results with the same twelve different initial momentum spreads but at high intensity(13×10^{11} protons) are shown in Figure 23. The impact of momentum spread can be easily compared on the same scale in Figures 22 and 23. Since the space charge effect is more significant in high intensity beams the impact of momentum spread on transverse emittance grow is enhanced compared to normal intensity.

The impact of initial momentum spread on the longitudinal beam properties at high intensity are shown in Figure 24.

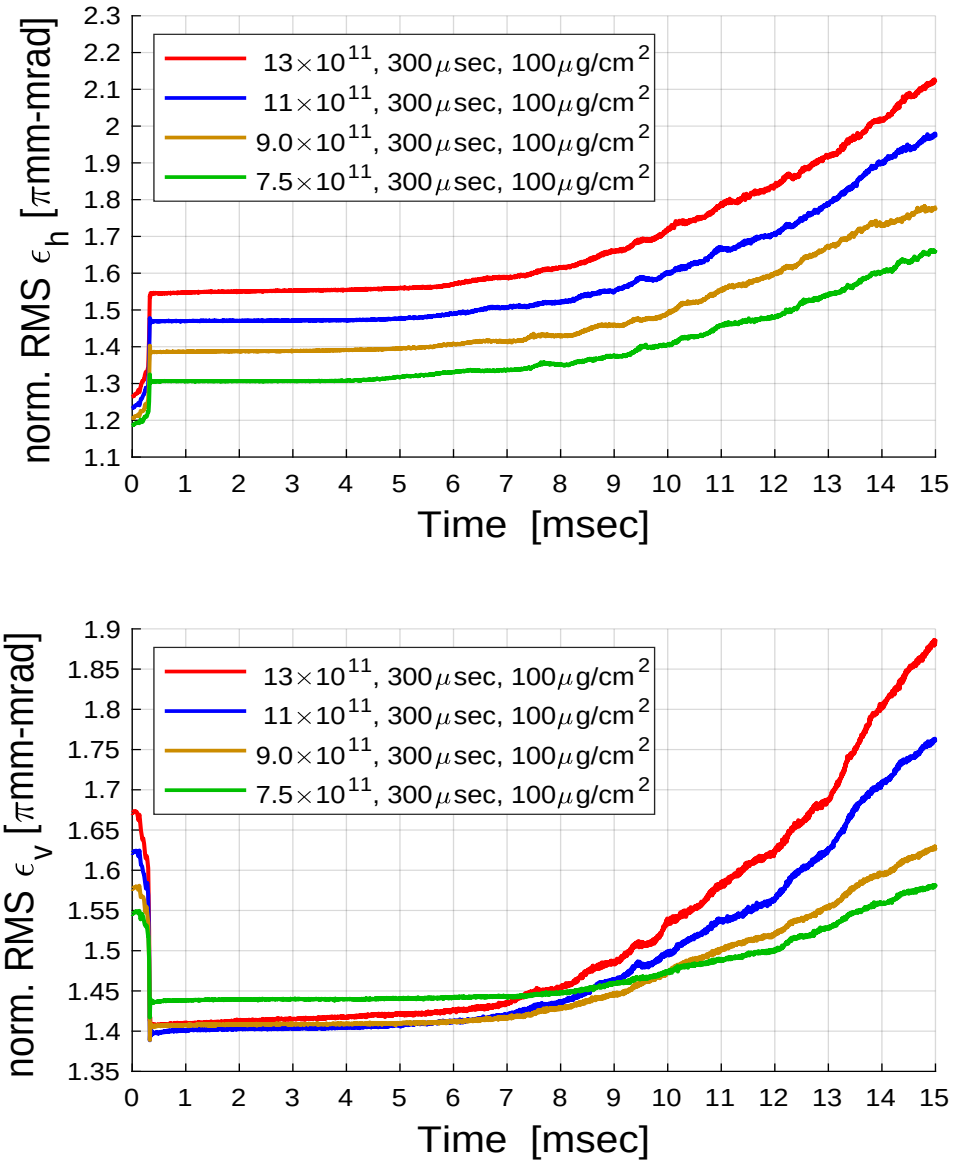

Figure 20: Horizontal (top sub-figure) and vertical emittance (bottom sub-figure) in beams with initial intensities of 7.5×10^{11}, 9×10^{11} 11×10^{11}. 13×10^{11} protons shown by breen, brown, blue and red curves, respectively.

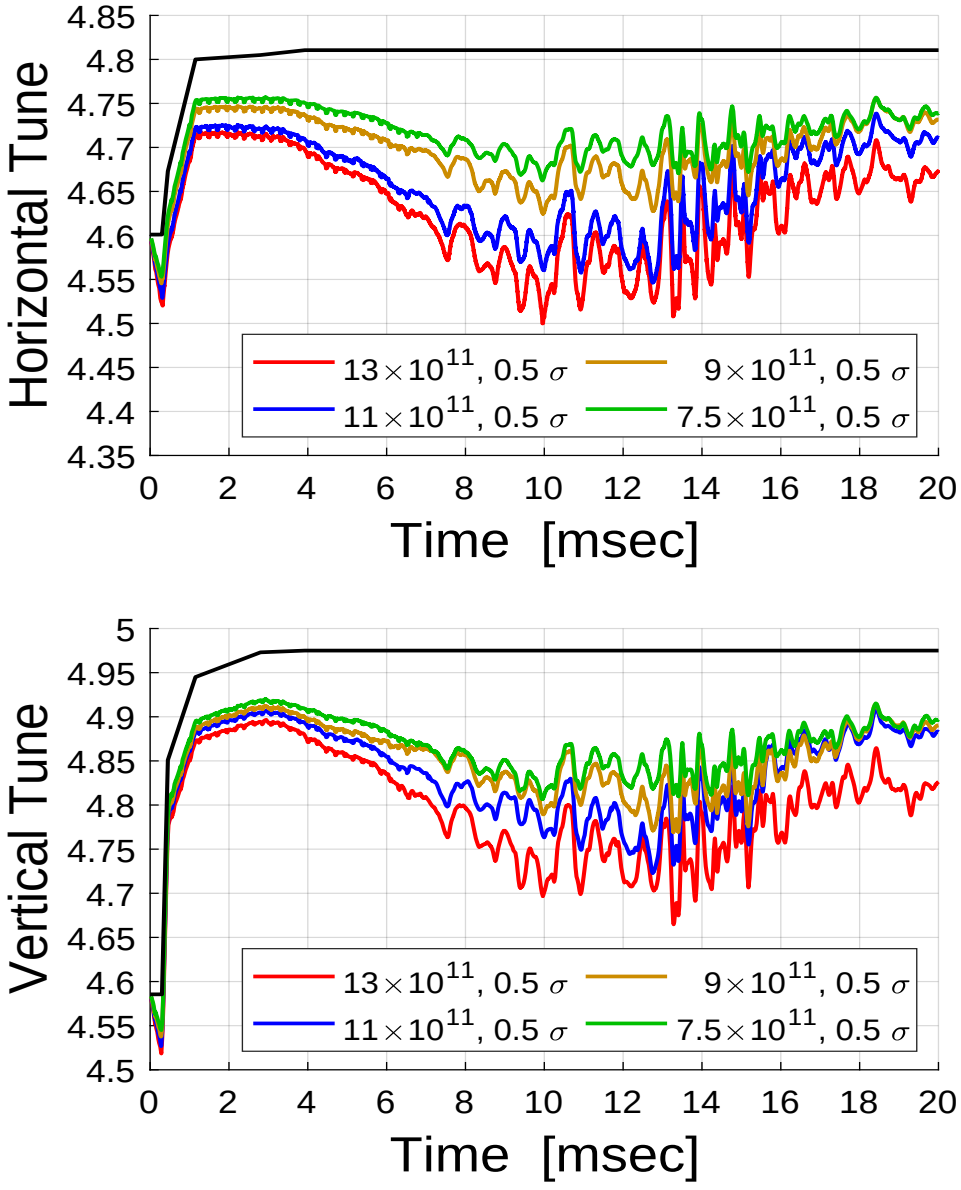

Figure 21: Horizontal and vertical tunes evolved in 4 different intensity beams (7.5×10^{11}, 9×10^{11}, 11×10^{11}, 13×10^{11} protons) during the early part of the Booster cycle. The black curves are the set-tune during the booster operation.

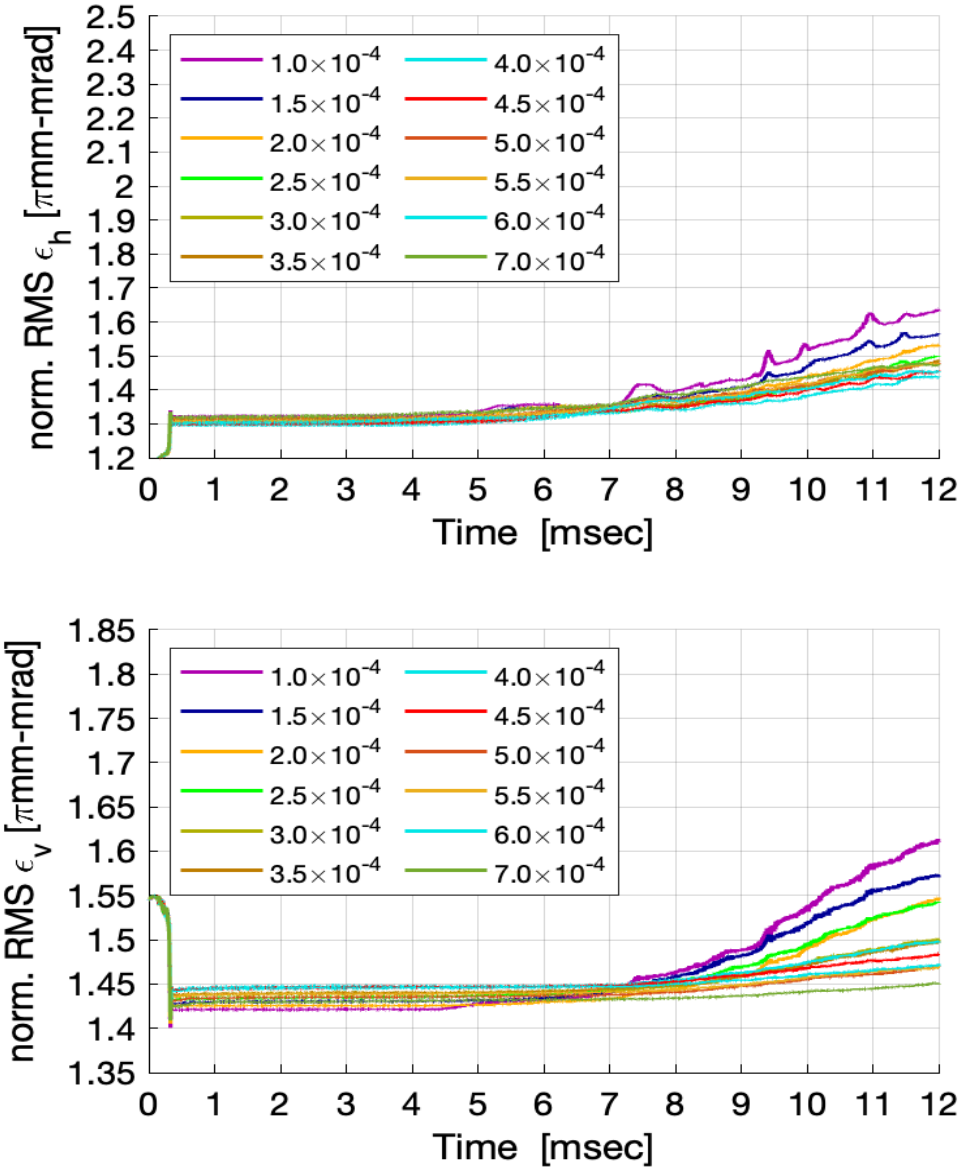

Figure 22: Horizontal and vertical emittance developed from 12 different initial momentum spread in the injected Beams of normal intensity (7.5×10^{11} protons).

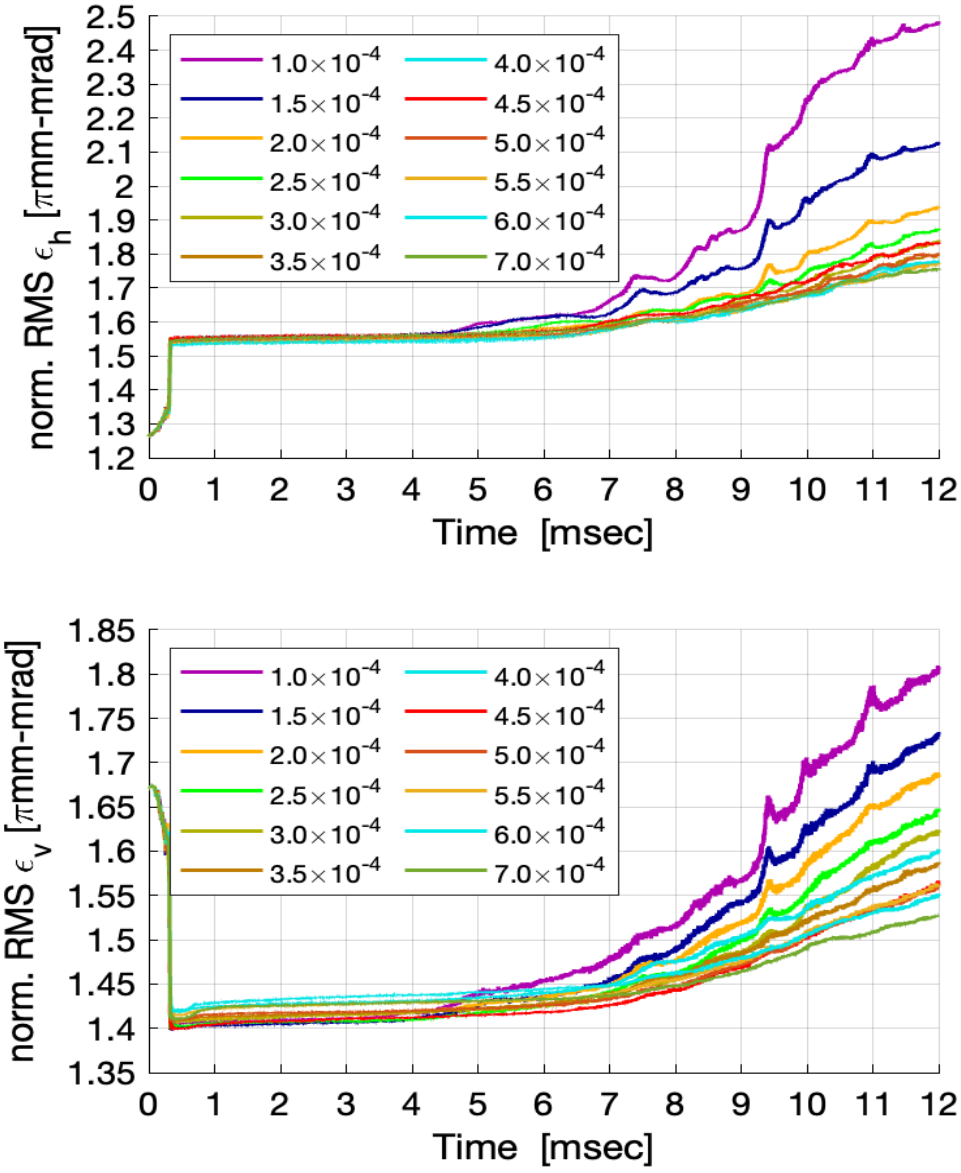

Figure 23: Horizontal and vertical emittance developed from 12 different initial momentum spread in the injected Beams of normal intensity (13×10^{11} protons).

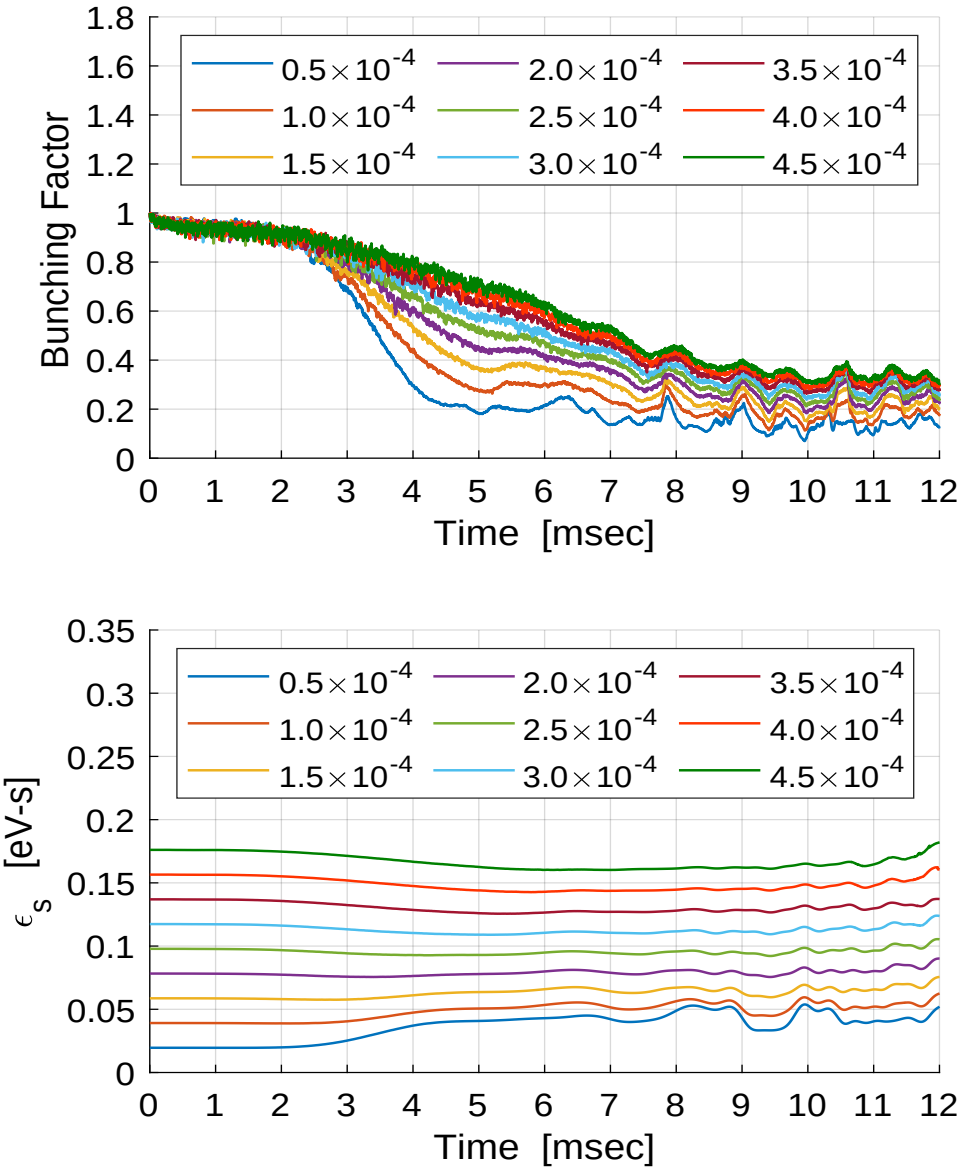

Figure 24: Bunching factor, longitudinal emittance and beam loss developed in the beams with 9 different initial momentum spread of (1, 1.5, 2, 2.5, 3, 3.5, 4, 5, 6)$\times 10^{-4}$ of high beam intensity (13×10^{11} protons).

6 Property Trends in High Intensity Beams

It would be helpful if quantitative relationships can be established between the injected and extracted beams. In this section, we explore the trends in beam properties during the evolution of high intensity beams through a full Booster cycle. The process has been to carry out a sequence of simulations where the only difference is the initial value of the single beam parameter under investigation. All other initial properties and machine conditions are kept the same for each simulation in the group.

In order to obtain the direct comparisons, the same operational settings, shown in Figure 25, are used for all groups of simulations. the top graph shows the magnetic field B and dB/dt during normal Booster energy ramping. The RF voltages of the 1^{st} and 2^{nd} harmonics, shown in the middle graph are extracted from the operational setting points during a typical Booster cycle. The relative phase of the 2^{nd} harmonic in relation to the 1^{st} RF harmonic is shown in the bottom graph. The red curve is from calculation, while the blue curve is extracted from the read-back scope during a typical Booster operation. Considering the run-time measurement is closer to reality, the blue curve is used in the simulations. The data points beyond the values provided by the blue curve were estimated by extrapolation.

In each full cycle simulation, an incident H^--beam with specified emittance and momentum spread $\Delta p/p$ is injected through a carbon foil of given thickness and tracked through the full cycle of the booster under space charge corresponding to the specified beam intensity.

The trend of the beam property change can be identified by comparing the final value (represented by the value averaged over the last 1 msec before extraction) with the initial value plotted on the same graph. Every such final value is the result of beam evolution through a Booster cycle starting with a specific set of beam property parameters, such as intensity, emittance and $\Delta p/p$. In this way, a one-on-one relationship between injected and extracted beams for the given set of machine conditions is established.

Figures 26 and 27 show the trends in horizontal and vertical emittance, respectively. In these two figures, simulations are grouped by four different

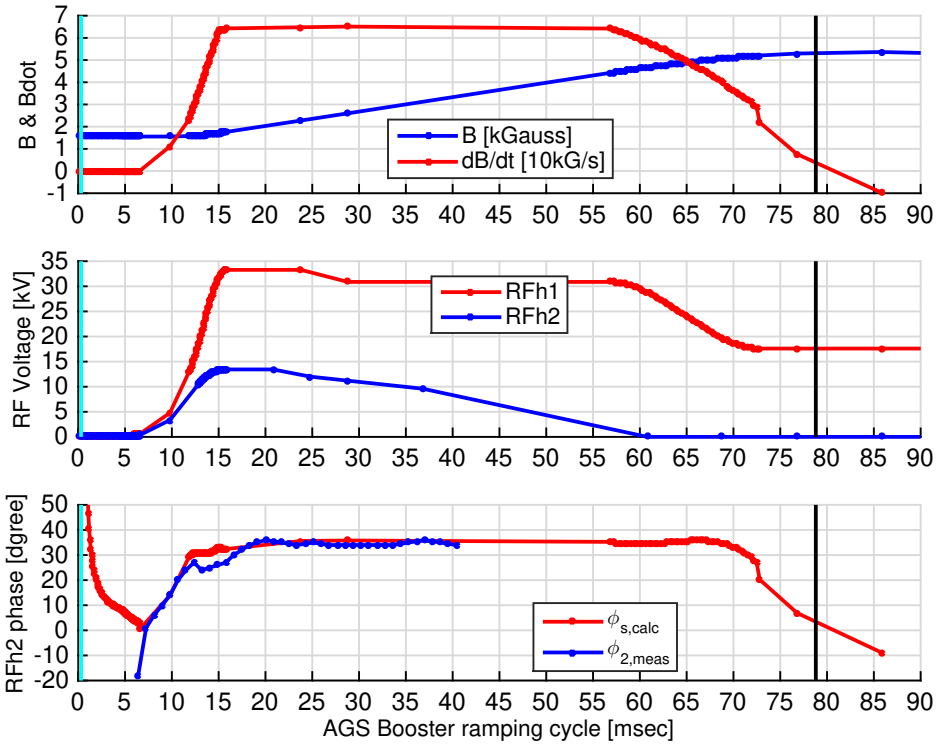

Figure 25: Some physical parameters used in the simulation of proton evolution during a Booster cycle. Top graph: magnetic field B and dB/dt; middle graph: the RF voltages of the 1st and 2nd harmonics; bottom graph: synchronous phase and relative phase of the 2nd harmonic. The red curves are from calculation; blue curves from the read-back scope during operation.

beam intensities first. They are plotted into sub-figures labeled by the value of the initial intensity, $N_{\rm init} = (7.5, 9, 11, 13) \times 10^{11}$. The simulations are further grouped into four sub-groups represented by different colors within each group. Each simulation within a sub-group has the same initial transverse emittance corresponding to injection foil thickness of 75,100, 135 and $200\,\mu{\rm g/cm}^2$ respectively. The transverse emittance at extraction (averaged over the last 1 msec) obtained from one simulation is plotted as one point

against its initial $\Delta p/p$. Each colored curve is obtained from the data points within each sub-group by applying a second-order polynomial fit.

Trends in longitudinal emittance, bunching factor and accumulated beam loss at extraction are shown in Figure 28. Groups of simulations are color-coded according to the four different values of N_{init}, and, as above, data points provide the input for second-order polynomial fits.

With the aid of the trend graphs in Figures 26 to 28 one will be able to predict likely extracted beam properties from the injected beam parameters. We take one case as an example. Assume the Booster is in the operation with injection pulse length 300 μsec and uses a charge exchange foil with thickness of 100 μg/cm^2. If a beam is injected with an initial intensity of $N_{\text{init}} = 9\times10^{11}$ and momentum spread $\Delta p/p = 3 \times 10^{-4}$, we get the estimated horizontal and vertical emittance of the extracted beam to be about 3.7πmm-mrad and 2.1πmm-mrad, respectively. These predictions are obtained by reading the value on y-axis where $\Delta p/p = 3 \times 10^{-4}$ on x-axis along the green curve in upper right sub-figure of Figures 26 and 27. Similarly, from Figure 28 we get the estimated longitudinal emittance, bunching factor and accumulated beam loss of the extracted beam to be 15 meV-s, 0.17 and 0.5% (excluding beam loss at the foil and emittance reduction operation by scraping).

Note that these simulations do not include magnet errors, noise and mismatch that may exist in the real machine. They do, however, include unavoidable numerical rounding and other errors and noise because of the limited number of macro-particles. With these provisos, these trend graphs can be used to quantify the evolution of well-behaved beams in a well-tuned Booster, effectively identifying a "best case scenario".

The ideas put forward in this section could provide an AI system that can be built into a system controlling machine operation through machine learning based on a rich and varied knowledge of Booster characteristics and parameter behavior.

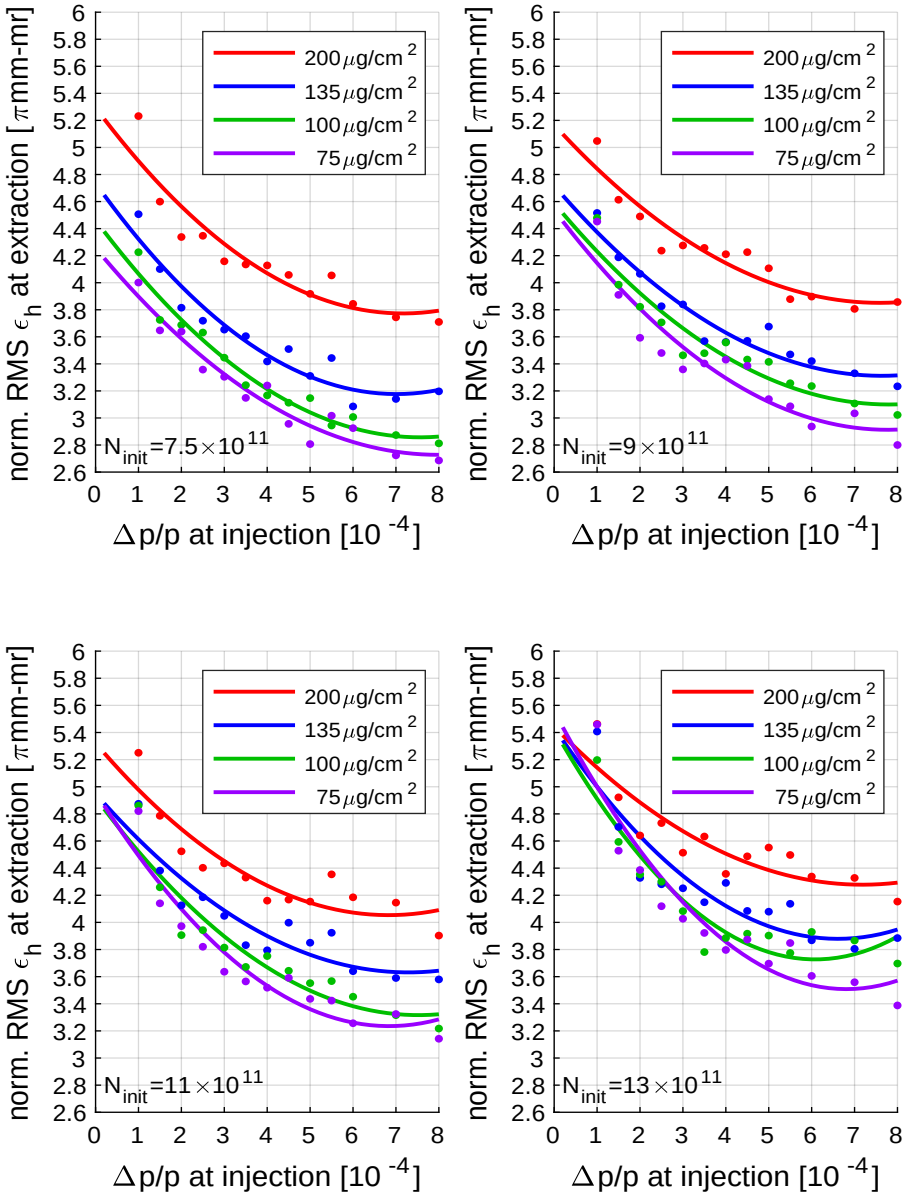

Figure 26: Trend in horizontal emittance of high intensity beams at extraction for varying initial $\Delta p/p$ with initial intensities of $N_{\text{init}} = (7.5, 9, 11, 13) \times 10^{11}$. The purple, green, blue and red curves are the 2$^{\text{nd}}$ order polynomial fits of extraction data obtained from injections using foil thicknesses of 75, 100, 135 and 200 μg/cm^2 respectively.

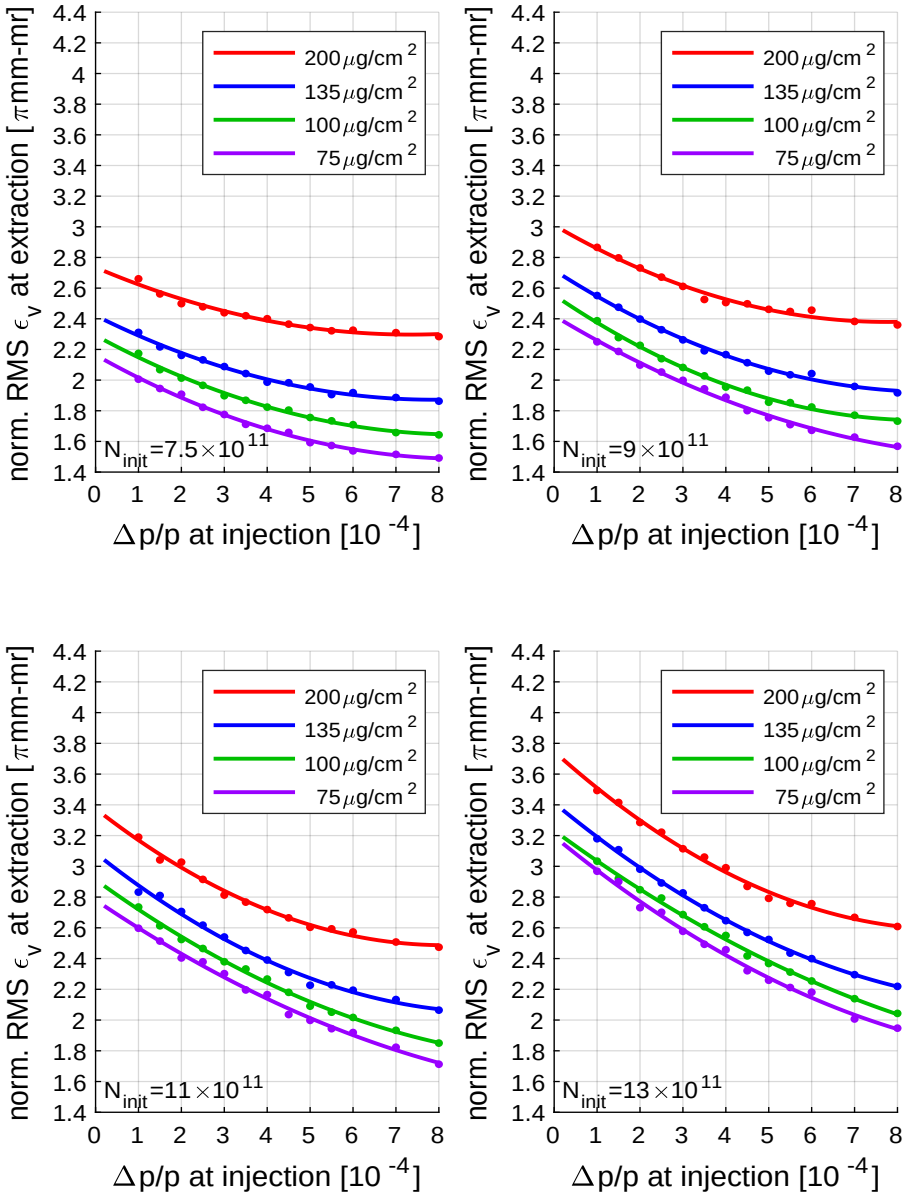

Figure 27: Trend in vertical emittance of high intensity beams at extraction for varying initial $\Delta p/p$ with initial intensities of $N_{\text{init}} = (7.5, 9, 11, 13) \times 10^{11}$. The purple, green, blue and red curves are the 2^{nd} order polynomial fits of extraction data obtained from injections using charge exchange foil thickness of 75, 100, 135 and 200 μg/cm^2, respectively.

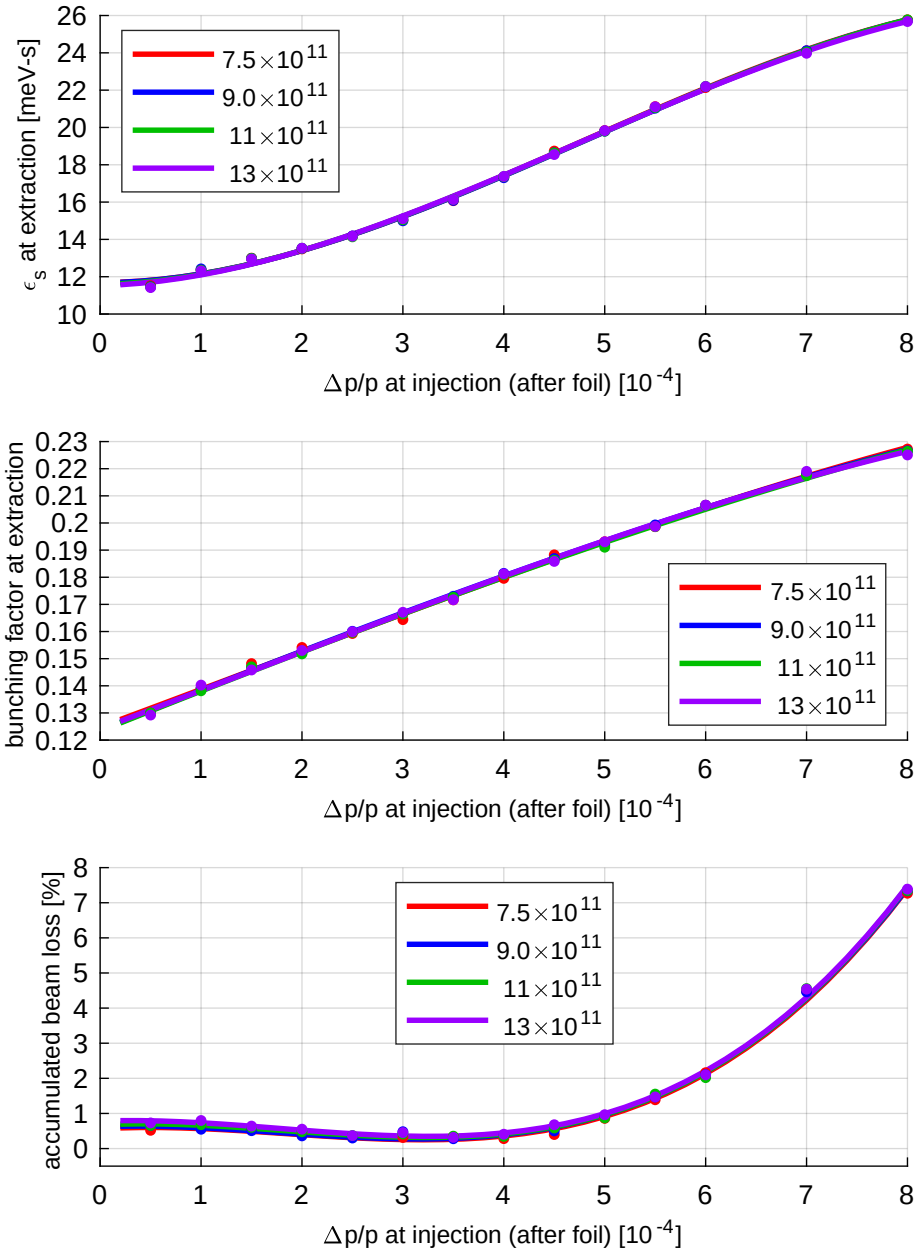

Figure 28: Trends in longitudinal emittance, bunching factor and accumulated beam loss at extraction for varying initial $\Delta p/p$ with initial intensities of $N_{\text{init}} = (7.5, 9, 11, 13) \times 10^{11}$.

7 Summary and discussion

Investigations into dynamics in the high intensity Booster beams have been performed using computer simulations including space charge, allied to known parameters and features of the machine.

The investigation is split into two major parts. The first covers beam injection and the early stages of the Booster cycle where focus is to investigate the impact of higher Intensity, longer pulse length and charge exchange foil thickness in the effort of pushing for higher intensity into the Booster. The second part concerns modeling of the full Booster cycle with realistic operational settings or run-time read-backs during the Booster operation. The aim here was to find the trends in changing beam properties through a full cycle by establishing quantitative relationships between parameters in the injected and extracted beams.

These studies have essentially been based on the Booster as it presently operates and trying to identify sources of beam loss and emittance growth. Further studies might consider finding theoretical alternative procedures to try to reduce the loss, whether through direct operating procedures or through mechanisms designed to improve parameter stability against progressive effects (mostly space charge effect). A revised RF voltage ramp and the 2^{nd} to 1^{st} harmonic phase variation could reduce the longitudinal beam loss resulting from particles finding their way out of the RF bucket. A revised orbit bump program at injection could reduce the number of protons traversing the injection foil, thereby reducing foil heating and improving foil lifetime. A revised foil thickness might improve stripping efficiency and reduce the effects of scattering.

Some ideas are amenable to experiment in the Booster ring; others can only be studied using simulation. The simulation runs may need to be repeated with a greatly increased number of macro-particles ($> 10^6$). The modeling here has looked mainly at RMS effects and the number of particles used is inadequate to study halo formation, non-linear space-charge effects and the onset of instabilities in detail.

The approach of finding the trends of beam property changes during evolution

by establishing quantitative relationships between parameters at different times, proposed in §6 has potential beyond this simulation study. An AI (artificial intelligence) system could conceivably be developed at real time and used to guide accelerator operations.

References

[1] I. Hofmann, "Space Charge Physics for Particle Accelerators", Springer (2017)

[2] J. Beebe-Wang, "Simulation of Proton Beams in the AGS Booster with Space Charge", BNL-224790-2023-TECH, C-A/AP/700 (2023)

[3] S. Machida, "Benchmarking and Application of Space Charge Codes for Rings", Proceedings of IPAC15, p2402-2407, Richmond, VA, USA (2015)

[4] "Booster-Design-Manual", AGS Booster Project, BNL, (1989) https://www.bnl.gov/cad/accelerator/docs/pdf/boosterdesignmanual.pdf

[5] D. Raparia, et al, "Polarized ion sources at BNL", Proceedings of Science, 25th International Spin Physics Symposium, Pos(SPIN2023)222, Durham, NC, USA (2023)

[6] K. Zeno, Booster-AGS-pp Elog, Entry 2015 Feb 13, 13:34, BNL, (2015)

[7] K. Zeno, Booster-AGS-pp Elog, Entry 2022 Apr 13, 17:15-17:19, BNL, (2022)